OPTICAL DESIGN OF A FIBER-FED IFU SPECTROGRAPH FOR THE DAG TELESCOPE

A THESIS SUBMITTED TO
THE GRADUATE SCHOOL OF NATURAL AND APPLIED SCIENCES
OF
MIDDLE EAST TECHNICAL UNIVERSITY

BY

TARIK SİPAHİ

IN PARTIAL FULFILLMENT OF THE REQUIREMENTS
FOR
THE DEGREE OF MASTER OF SCIENCE
IN
PHYSICS

SEPTEMBER 2023

Approval of the thesis:

OPTICAL DESIGN OF A FIBER-FED IFU SPECTROGRAPH FOR THE DAG TELESCOPE

submitted by **TARIK SİPAHİ** in partial fulfillment of the requirements for the degree of **Master of Science in Physics Department, Middle East Technical University** by,

Prof. Dr. Halil Kalıpçılar
Dean, Graduate School of **Natural and Applied Sciences** _____

Prof. Dr. SEÇKİN Kürkcüoğlu
Head of Department, **Physics** _____

Assoc. Prof. Dr. Sinan Kaan Yerli
Supervisor, **Physics Department, METU** _____

Examining Committee Members:

Prof. Dr. Selim Osman Selam
Astronomy and Space Sciences Department, Ankara University _____

Assoc. Prof. Dr. Sinan Kaan Yerli
Physics Department, METU _____

Assist. Prof. Dr. Ihor Pavlov
Physics Department, METU _____

Prof. Dr. Hakan Altan
Physics Department, METU _____

Prof. Dr. Alpan Bek
Physics Department, METU _____

Date:05.09.2023

I hereby declare that all information in this document has been obtained and presented in accordance with academic rules and ethical conduct. I also declare that, as required by these rules and conduct, I have fully cited and referenced all material and results that are not original to this work.

Name, Surname: Tarık Sipahi

Signature :

ABSTRACT

OPTICAL DESIGN OF A FIBER-FED IFU SPECTROGRAPH FOR THE DAG TELESCOPE

Sipahi, Tarık
M.S., Department of Physics
Supervisor: Assoc. Prof. Dr. Sinan Kaan Yerli

September 2023, 68 pages

The main objective of this study is to provide an optical design of a spectrograph in the intermediate spectral resolution range ($\mathcal{R}$>1000) while ensuring a high optical throughput. The study explores the use of an integral field unit (IFU) that combines imaging and spectroscopy and generates the spectrum of two-dimensional content. For the IFU design, hexagonally packed microlens arrays are used which are followed by 61 fibers showing the best filling efficiency while enabling a spatial coverage of the broadest conceivable content. A code was developed to run Rigorous Coupled-Wave Analysis (RCWA) calculations to determine the optimum parameters of the volume-phase holographic grating that achieves high diffraction efficiency with the widest possible FWHM of spectral coverage. The code includes the calculation for the basic parameters of the spectrograph's optical elements and the results are verified over OpticStudio/ZEMAX software. The proposed design is finalized with three Volume-Phase Holograph Grating (VPH) based spectral arms covering the visible and near-infrared spectral regions.

Keywords: VPH Grating, Spectrograph, Optical Design, Instrumentation, Astronomy

ÖZ

DAG TELESKOBU İÇİN FİBER BESLEMELİ IFU TAYFÖLÇERİNİN OPTİK TASARIMI

Sipahi, Tarık
Yüksek Lisans, Fizik Bölümü
Tez Yöneticisi: Doç. Dr. Sinan Kaan Yerli

Eylül 2023 , 68 sayfa

Bu çalışmanın temel amacı, yüksek optik geçirgenliği sağlarken orta spektral çözünürlük aralığında ($\mathcal{R}$>1000) bir tayfölçerin optik tasarımını sunmaktır. Çalışma, görüntüleme ve spektroskopiyi birleştiren ve iki boyutlu içeriğin tayfını üreten bir Integral Alan Biriminin (IFU) kullanımını araştırmaktadır. IFU tasarımı için, akla gelebilecek en geniş içeriğin mekansal kapsamını mümkün kılarken en iyi doldurma verimliliğini gösteren 61 fiberin takip ettiği altıgen olarak paketlenmiş mikromercek dizileri kullanılır. Yüksek kırınım verimliliğini ve spektral kapsama genişliğinin mümkün olan en geniş FWHM'sini elde etmek üzere tasarlanmış bir kod geliştirilmiştir. Böylece VPH grating tasarımının en uygun parametreleri belirlenmiştir. Kod ayrıca tayfölçerin optik elemanlarının parametrelerinin hesaplamasını da içerir ve sonuçlar OpticStudio/ZEMAX yazılımı üzerinde doğrulanır. Önerilen tasarım, görünür ve yakın kızılötesi spektral bölgeleri kapsayan üç VPH (Volume-Phase Holograph Grating) tabanlı spektral koldan oluşmaktadır.

Anahtar Kelimeler: Holografik Grating, Tayfölçer, Optik Tasarım, Aygıtlar, Astronomi

To my uncle Sabir

ACKNOWLEDGMENTS

Part of this work was carried out in AOL (Astronomical Optics Laboratory) which was established within the framework of the DAG (Eastern Anatolian Observatory) project. AOL was established within the scope of the project titled “Eastern Anatolia Observatory Focal Plane Instruments and Adaptive Optics Systems” (2016K12-2857) under the Ministry of Development, Strategy Budget Department.

I would like to thank my advisor Dr. Yerli for his support and guidance throughout my master’s studies. He always welcomed new ideas that I came up with. I always walked out of his room motivated to learn and do more science.

The second person that the thanks should go to is my uncle Sabir. I used to help him in his workshop since I was a kid. He taught me how to handle and construct small parts of design and how to think like a scientist. Because of him, I chose the path of scientific instrumentation.

Although part of this study was during COVID-19 pandemic, I had the chance to participate in several scientific/social events organized by the student chapters of OPTICA/SPIE. One more place to thank is the Canteen of the Physics department. It was a great place to gather during this period. I want to thank Onur Şölen for his delicious coffee and catering.

I would like to extend my thanks to Astronomical Optics Laboratory team and my coworkers at Transvaro Electro-Optics for their support. Many thanks to my friends and colleagues: Dogukan Alkan, Yusuf Gabrah, Basil Eldeeb, Firat Idikut, Ujal Rzayev, Tunc Bektas, Giray Mecit, Ahmed Ouf Konan, Abdelaziz Emad, Ahmed Habib, Serhat Unal, Aburrahman Barudi, Mehmet Salduz, Alperen Tatarhan, Abdullah Mesut, Yasin Arslan, Mahmut Sinan Yayla, Ahmed Elghwel, Mehtap Fidan, Bartu Karaduman, Mohamed Saad, Cem Maden, Sinan Celik, Elif Gulen, Ata Tofig, Pouyan Sharafuddin, Dr. Tenay Saguner, Gunseli Cetin, Hande Cetin, and Cagdas Ulus.

TABLE OF CONTENTS

ABSTRACT v

ÖZ vii

ACKNOWLEDGMENTS x

TABLE OF CONTENTS xi

LIST OF TABLES xv

LIST OF FIGURES xvii

LIST OF ABBREVIATIONS xx

CHAPTERS

1 INTRODUCTION 1

1.1 Spectroscopy Through History 1

1.2 Astronomical Spectroscopy 2

1.3 Astronomical Instrumentation 2

1.4 Designing Instruments for Astronomy 5

1.4.1 Determination of Scientific Needs 5

1.4.2 Bringing Science and Engineering Together 5

1.4.3 Standard Photometric Systems 6

1.4.4 Importance of Spectroscopy in Astronomy 7

1.4.4.1 Hydrogen-Alpha Line H_α 8

1.4.4.2 Hydrogen-Beta Line H_β 9
1.4.4.3 Near-Infrared Observations 9
1.4.5 Optical Design 9
1.5 Eastern Anatolia Observatory (DAG) 10
1.5.1 Focal Plane Instrumentation (FPI) for DAG 11
1.6 Objectives of this work and Its organization 12
2 METHODOLOGY 15
2.1 Spectrograph Design 15
2.2 Optical Design of a spectrograph 17
2.2.1 Entrance Slit 17
2.2.2 Collimation 17
2.2.3 Disperser 18
2.2.4 Focusing Camera Optics 19
2.2.5 Charge-Coupled Devices CCD 19
2.3 Optical Design Process 20
2.3.1 The First Order Optical Design 21
2.3.1.1 Thin lens 22
2.3.1.2 Thick Lenses 22
2.3.2 Lagrange Invariant 23
2.3.3 Optical Throughput AΩ 23
2.3.4 Using Optical Design Software for Optimization 24
2.4 Geometrical Optics of a Spectrograph 24
2.5 Integral Field Spectroscopy 26

2.6 Fiber-Fed Spectroscopy 28
2.6.1 Focal Ratio Degradation (FRD) 29
2.6.2 IFU using Micro Lens Array (MLA) 30
2.6.3 Multi-Mode Fiber (MMF) Coupling Efficiency 31
2.6.4 Fore-Optics for Telecentric Magnification 31
2.6.5 Optical Design of a Telecentric Magnifier 31
2.6.6 Losses due to Non-Telecentricity 32
2.7 Volume-Phase Holographic Grating 33
2.8 Spectrograph Design Consideration 37
3 INTEGRAL FIELD UNIT (IFU) DESIGN 39
3.1 Introduction 39
3.2 First IFU Design using a Fiber Array 39
3.2.1 Paraxial Design for a Circular IFU array 41
3.2.2 Real Optical Design for the circular IFU fiber array 41
3.2.3 Optimization for Fiber Coupling Efficiency 42
3.3 IFU Design using MicroLens Array (MLA) 43
3.3.1 Geometrical Optics Calculations 44
3.3.2 Design Optimization 47
3.4 IFU Final Design 47
4 PHOTONIC DESIGN OF THE VOLUME-PHASE HOLOGRAPHIC GRATING 51
4.1 Blue Arm Design 52
4.2 Red Arm Design 53

4.3 Near-Infrared (NIR) Arm Design 54

5 SPECTROGRAPH OPTICAL DESIGN 57

5.1 Geometrical Optics Calculations 58

6 CONCLUSION 61

REFERENCES 65

LIST OF TABLES

TABLES

Table 1.1 Johnson Photometric System in Astronomy 7

Table 1.2 Optical Design of the DAG Telescope [1] 11

Table 3.1 IFU initial design parameters using a fiber array. 40

Table 3.2 Magnifier lens surface data. 42

Table 3.3 Results of filling the focal plane with a hexagonal grid. 44

Table 3.4 Microlens Array Design 46

Table 3.5 The hexagonal IFU design parameters. 47

Table 3.6 Surface table of the hexagonal IFU design. 48

Table 3.7 Final results of the IFU design. 48

Table 3.8 Final parameters of the IFU design. 49

Table 4.1 Optical Requirements for a Three-arm Spectrograph 52

Table 4.2 VPH Final Parameters for the Blue Arm. λ_c: Central Wavelength; $\Delta\lambda$: Wavelength Range; ν: Spatial Frequency; t: Grating Thickness; Δn: Sinusoidal Modulation; α: Blaze Angle. 53

Table 4.3 VPH Final Parameters for the Red Arm. λ_c: Central Wavelength; $\Delta\lambda$: Wavelength Range; ν: Spatial Frequency; t: Grating Thickness; Δn: Sinusoidal Modulation; α: Blaze Angle. 54

Table 4.4 VPH Final Parameters for the NIR Arm. λ_c: Central Wavelength; $\Delta\lambda$: Wavelength Range; ν: Spatial Frequency; t: Grating Thickness; Δn: Sinusoidal Modulation; α: Blaze Angle. 56

Table 5.1 Requirements for the desired spectrograph. 58

Table 5.2 Optical system parameters for the three-arm design. 59

LIST OF FIGURES

FIGURES

Figure 1.1 Basic flow chart of astronomical instrument design. 4

Figure 1.2 Layout for the Optics of the DAG Telescope with Two Nasmyth Foci 12

Figure 2.1 The summary of the optical design process of a spectrograph. . . 20

Figure 2.2 The summary of the optical design process involving an integral field spectrograph. 21

Figure 2.3 (Upper Panel) Optical throughput and cone of rays where A represents the area and Ω represents the solid angle. (Bottom Panel) Optical invariant where h is the chief ray height and θ is the marginal ray angle and the optical invariant for the finite-conjugate systems is equal in both the object and image space as $n_1 h_1 \theta_1 = n_2 h_2 \theta_2$. 24

Figure 2.4 Basic Optics of a Spectrograph Based on Thin Lens Paraxial Approximation (Adapted from [2]). 25

Figure 2.5 Schematic explanation of integral field spectroscopy (adapted from [3]). 27

Figure 2.6 Focal ratio degradation and the change in the f-number. 29

Figure 2.7 Focal ratio degradation and the change in the f-number in real cases (adapted from [4]). 30

Figure 2.8 Light propagation through a single microlens and the effect of telecentricity on the coupling efficiency 33

Figure 2.9 Light passing through the VPH surfaces, the width of the DCG is not to scale 35

Figure 2.10 Sinusoidal variation of the refractive index according to Littrow Configuration, where the grooves are parallel to the optical axis (top-left panel). The grooves have slanted angle to the optical axis (top-right panel). The depth of variation of the refractive index on the z-axis (bottom panel). 36

Figure 3.1 Filling the fibers at the magnifier focal plane. 40

Figure 3.2 First-order magnifier lens for the initial design. 41

Figure 3.3 Real Optical Design of the Telecentric Magnifier Lens Before the Circular Fiber Array 42

Figure 3.4 Results of optimization for multi-mode coupling efficiency. . . . 43

Figure 3.5 Light passing through a single microlens 43

Figure 3.6 Physical look of filling the focal plane with a hexagonal grid. . . 45

Figure 3.7 Final surface sage of hexagonal lens array with hexagonal packing using Zemax. 49

Figure 4.1 Blue Arm diffraction efficiency: (top-left panel) With respect to the sinusoidal refractive index. (top-right panel) With respect to the grating thickness. (bottom panel) With respect to the wavelength. 53

Figure 4.2 Red Arm diffraction efficiency: (top-left panel) With respect to the sinusoidal refractive index. (top-right panel) With respect to the grating thickness. (bottom panel) With respect to the wavelength. 55

Figure 4.3 Near-Infrared (NIR) Arm diffraction efficiency: (top-left panel) With respect to the sinusoidal refractive index. (top-right panel) With respect to the grating thickness. (bottom panel) With respect to the wavelength. 56

Figure 5.1 1D fiber array slit (left) and dispersed spectra along spatial direction as seen by a CCD camera (right). 57

Figure 5.2 Variation in collimator focal length and the resulted spectral resolution and Airy disk. 59

LIST OF ABBREVIATIONS

CCD	Charge-Coupled Device
DAG	Doğu Anadolu Gözlemevi (Eastern Anatolia Observatory)
FPI	Focal Plane Instrumentation
FWHM	Full-Width at Half Maximum
IFS	Integral-Field Spectroscopy
MLA	Micro-Lens Array
MOS	Multiple-Object Spectroscopy
RCWA	Rigorous Coupled Wave Analysis
SNR	Signal-to-Noise Ratio
UDA	User-Defined Aperture
VPH	Volume-Phase Holographic Grating

CHAPTER 1

INTRODUCTION

1.1 Spectroscopy Through History

Spectroscopy started with Ibn Al-Haytham when he performed his first experiment on dispersion. He allowed sunlight to pass through a water-filled globe and observed the constituent colors of the incident light [5, 6]. Newton followed Ibn Al-Haytham by performing his popular experiment on dispersion using a glass prism to split white light into component colors [7].

Back in the 18th century, Fraunhofer demonstrated the reason behind dark spectral lines in the Sun's spectrum. The dark lines were connected to absorption by chemical elements in the Sun's atmosphere. This was when scientists grasped the idea that the spectrum we get from stars can give information about their chemical composition and answer the popular question of how stars are made [8].

From there on, scientists started to construct a profound understanding of the relationship between the spectrum of objects and their chemical composition. By knowing the distinctive pattern of each chemical element in the lab, scientists can identify these lines from observed objects in the sky. Breaking the emitted beams from celestial objects down into their constituent wavelengths and comparing them with the chemical signature of elements has formulated today's astronomical spectroscopy [9]. Sometimes, however, the sequence went in reverse. For instance, Helium was first discovered by looking at the spectrum of the chromosphere of the Sun before the elements were seen on Earth [10].

The first spectroscope was made by Kirchhoff and Bunsen in 1860 for chemical anal-

ysis based on spectral observations [11]. In 1880, Gustav Wiedemann continued their journey by revealing many other details hidden inside the Sun's spectrum such as temperature, pressure, and density of the layers of the Sun's atmosphere. In 1897, Pieter Zeeman Suggested the potential of measuring stellar magnetic fields [12].

1.2 Astronomical Spectroscopy

Spectroscopy plays a significant role in gaining knowledge of stars, galaxies, and many celestial phenomena. The spectra of celestial objects reveal much information about the emitting object. Many other properties of celestial objects can be derived by just analyzing their spectra: chemical composition, distance, mass, temperature, motion, luminosity, and other possible physical properties.

1.3 Astronomical Instrumentation

Since the beginning of civilization, humans wondered voraciously about the sky, trying to understand the vastness of the universe and our place within it. Wondering about the sky started by developing some basic tools such as the astrolabe in ancient civilizations. This was considered the first astronomical instrument used by humankind. In the last three decades, astronomical instruments have been advancing in a very exponential way. This was due to the advancing technology that curious astronomers were catching up with. The continuous developments and advancements accumulated our understanding of the universe and shaped the science of today's astronomy. However, this would never be possible or even imaginable without having larger and more powerful telescopes like those existing today.

Galileo crafted his own simple telescope in his workshop to watch and observe celestial objects. Therefore, he changed our understanding of the universe surrounding us. However, the age of becoming an astronomer as Galileo has gone by. Modern ground-based optical telescopes require tools that take years of continuous development, consume a long time for engineering, and ultimately require extravagant budgets to manufacture. In that sense, a considerable amount of financial resources, long

periods of development, and investments in cutting-edge technologies are required to contribute to advancing this scientific discipline.

In the last two decades, there has been a remarkable rise in the complexity of general scientific instrumentation particularly in the field of astronomy. This trend is also evident in ground-based instrumentation. For instance, starting from the 1990s, the minimum development time of an instrument for an 8-meter class telescope demands around eight years, a period that involves considerable financial investments for implementation, manufacturing, as well as design, engineering and labor costs [13]. To tackle the problem of the increased complexity of instrument development, both scientists and engineers spend more time in simulations before the implementation stage with the help of high-performance computing. For example, the developments of software tools and libraries have emerged as significant strategies for controlling this increase. In addition to these approaches, incorporating advanced simulation tools such as OpticStudio/ZEMAX software for optical design and image quality analyses has become crucial in every part of the design stages. These technologies allow both scientists and engineers to simulate real-world conditions and performance and further optimize designs before physically constructing instruments. Furthermore, implementing rapid prototyping through techniques such as 3D printing has expedited the refining of instrument components' design and assembly processes.

Furthermore, manufacturability of an instrument should always be kept in mind while designing an instrument. The design is expected to not exceed any certain constraints or diverge from the scientific needs it is meant to fulfill. Note that the final product has to improve observations and capabilities mentioned by the scientific community. The instrument is meant to exceed the limits that the community has already reached by creating new cutting-edge tools.

A basic flow chart of astronomical instrument design is summarized in Figure 1.1 and in the latter sections each stage is described in detail.

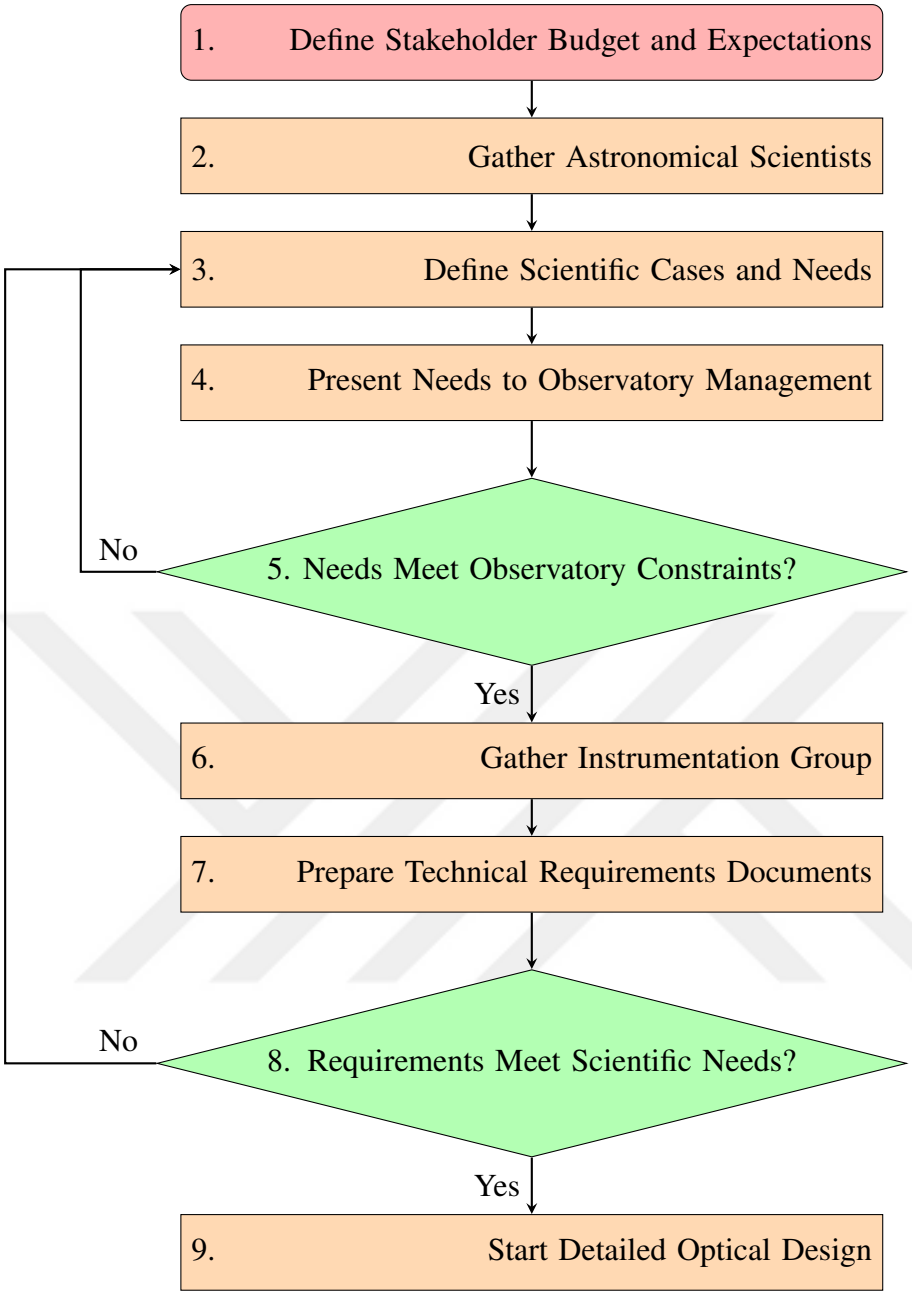


Figure 1.1: Basic flow chart of astronomical instrument design.

1.4 Designing Instruments for Astronomy

1.4.1 Determination of Scientific Needs

Development of novel scientific instruments is no longer the job of a single person or even a small group of specialists. It requires active communication between astronomers, engineers and designers to work together. Extensive discussions must be carried out to decide on scientific needs for novel instruments. The needs may vary according to the device specifications and scientific objectives. Usually, the kick-off meetings involve astronomers, project managers and people working at the observatory. This is important in order to define the limits of the current devices and the prospective next-generation ones to be developed. Scientific needs have to be defined clearly such that the development process can easily be evaluated according to the final milestone. At this stage, people from different disciplines may not be involved as the scientific needs may not reflect any technicalities for the design team. Afterward, scientists finalize the following variables, which should be fixed before the production stage: Resolution, field of view, sensitivity, throughput, and constraints such as mechanical dimensions, temperature, wavelength range, seeing limit, and diffraction limit. Technical teams may not well understand some of the defined parameters. That is why the next stage of system engineering is essential to define the roadmap for building such an instrument and ensure that the final product meets the scientific requirements defined at this stage. Meeting these requirements will result in a spectrograph enabling the latest state-of-the-art research and significantly contributing to our understanding of the universe.

1.4.2 Bringing Science and Engineering Together

The right combination of science and engineering is essential in developing new scientific tools. Any miscommunication of the scientific needs between the two parties may lead to unmet technical requirements, ultimately at a very high cost. This stage usually involves systems engineering, where scientists and engineers communicate. Finding a technical partner who understands the perspective system as a whole and writes down the technical requirements document for designing the instrument is one

of the most challenging steps. It is hard because sometimes scientists and engineers do not speak the same jargon due to astronomical projects' complexity and interdisciplinary nature. Furthermore, a systems engineer would develop a system architecture design by understanding each subsystem required and its life-cycle from designing and testing till final evaluation and then verification.

All the shared partners including astronomers, scientists, engineers and project managers work together to determine each subsystem with the specific features needed, performance parameters required and constraints of the instrument to be met. The requirements are based on the scientific objectives, targeted sky objects and the desired outcomes of the instrument. The function of systems engineering is to address technical challenges, assess risks and establish project management processes.

Building any astronomical instruments starts by discussing the scientific needs as mentioned before. In astronomical spectroscopy it is the job of astronomers to determine the scientific outcomes from the designated device. After that, physicists, designers and engineers meet to define the system requirements such as wavelength range, central wavelength, spectrograph's field of view, spectral resolution, resolving power, SNR (signal-to-noise ratio), encircled energies, throughput, sensitivity and stray light. These requirements should already be revised according to the optical manufacturers and the commercial-off-the-shelf products of lenses, mirrors and CCDs.

In this part of this study, an extensive literature survey was done to examine the best system requirements that can bring the most possible scientific outcomes with certain constraints on budget.

1.4.3 Standard Photometric Systems

Photometric systems are a series of well-predefined optical filters or pass-bands with predetermined sensitivity to a particular incident radiation. This sensitivity is dependent on the photodetectors, filters and other optical elements in use. Standard photometric systems have been revolutionized after photodetectors improved by increasing their sensitivity, transmission wavelength range and further. It is totally based on the

advancements in optics and photodetection [14].

One of the most popular systems known in astronomy is the Johnson system (see Table 1.1 for details). For example, the Johnson-B is used to measure the bluish light that shines from celestial objects like stars or galaxies. Color of celestial objects reflects the temperature of emission. Thus, the more we shift the filters from ultraviolet to mid-infrared, the cooler the objects that we can observe. That's why, for hot stars, observers tend to use ultraviolet filters and photodetectors [15].

Table 1.1: Johnson Photometric System in Astronomy

Filter	$\lambda_{central}$ (nm)	$\Delta\lambda$ (nm)	Description
U	365	68	Ultraviolet
B	445	94	Blue
V	551	88	Visual
R	658	138	Red
I	806	149	Near-Infrared (NIR)
J	1220	213	Near-Infrared (NIR)
H	1630	307	Near- Infrared (NIR)
K	2190	390	Near-Infrared (NIR)
L	3450	472	Near-Infrared (NIR)
M	4750	460	Mid-Infrared (MIR)
N	10500	2500	Mid-Infrared (MIR)
Q	20500	5800	Mid-Infrared (MIR)

1.4.4 Importance of Spectroscopy in Astronomy

By knowing the spectral fingerprint of each chemical element, scientists can define the chemical composition of celestial objects. This is done by analyzing the spectrum of the light emitted from distant objects and matching it with the elements' fingerprints of both emission and absorption lines. The spectra are produced by a transition

from different energy levels at the atomic scale. For example, the emission spectrum of hydrogen consists of several spectral series. They reflect the electron transitions between the electron energy levels in the atom. The hydrogen spectral series are known by the scientists who discovered them. They are known by Lyman, Blamer, Paschen, Brackett, and Pfund.

The Balmer series, however, has special importance in astronomy. Their spectral lines are bright and appear in several stellar objects compared to other spectral lines. This is because of the abundance of hydrogen in the universe. Balmer lines can be used to determine the surface temperature, surface gravity and composition of celestial objects which is dependent on the strength of these spectral lines. They are used in the determination of the radial velocities of celestial objects by looking at their Doppler shift. Using these shifts astronomers understand and detect various objects such as binary stars and exoplanets. Even compact objects such as neutron stars and black holes can be detected using Balmer lines by observing the kinematics of disks surrounding these objects [16]. In addition to this, it can help in determining the distance of galaxies and quasars by their redshifts [16].

Some important spectral lines are introduced and their astronomical importance are given below.

1.4.4.1 Hydrogen-Alpha Line H_α

H_α is a powerful tracer of ionized gas and star formation. The H_α emission occurs when the electron leaves the energy level of n=3 and jumps back to the second energy level n=2. During this emission, a photon is radiated with a wavelength of λ=656.279 nm. It happens when the hydrogen atom is ionized. That's why it is considered the most convenient indicator in the detection of ionized hydrogen content in gas clouds.

- **Nebula Cloud :** As Hydrogen is the primary and most abundant component of nebulae, H_α line can indicate the shape and extent of the Nebula cloud [17].
- **Star Formation Rate (SFR) Indicator :** The H_α luminosity is related to the radiation of massive stars. Several studies have shown a direct correlation between the luminosity of H_α emissions and the star formation rate [17].

- **Active Galactic Nucleus AGN :** These are active super-massive black holes at the center of their galaxy, which are responsible for the emission of bright jets and winds. They usually shape their galaxy [18].

In short, the H_α emission can indicate several astronomical phenomena and help astronomers in their quest for understanding star formation, black holes, and the dynamics of interstellar mediums.

1.4.4.2 Hydrogen-Beta Line H_β

The astronomical importance of the H_β spectral line is similar to the H_α line. It is the second line in the Balmer's emission spectrum. The H_β emission occurs when the electron leaves the energy level of n=4 and jumps back to the second energy level n=2. During this emission, a photon is radiated with a wavelength of λ=486.135 nm. This line has an important role for example in determining the redshifts of quasars. It gives details about the expansion in the universe and the distance to the very far objects known by cosmic distance [19].

1.4.4.3 Near-Infrared Observations

In astronomy, radiation from the NIR band (Johnson-J, 1.1-1.4 μm, centered on 1.25 μm) is used to study the atmospheres of cool stars, molecular clouds, which are significant for the study of star formation. The J-band is useful for ground-based observatories to access the sky because electromagnetic radiation in this spectral range can pass through Galactic clouds and other atmospheric gases. In this spectral range, there is a footprint of several atoms and molecules as well [20].

1.4.5 Optical Design

The optical design stage is critical to astronomical instrumentation, mainly telescopes, and spectrographs. Optical design starts from basic conceptual design using a first-order paraxial approximation to realistic optics. This includes choosing the optical

elements appropriately for the purposes of the system. Optical elements may include lenses, mirrors, filters, grating, dichroic surfaces, etc. After choosing a certain configuration of optical elements, an optical software program such as OpticStudio/ZEMAX is used for system optimization, quality, mechanical tolerances, and stray light analysis.

Optical devices must be developed and manufactured in accordance with criteria and goals in order to perform properly. The type of optical device and its use may alter the requirements for building that system. The following are some common optical design requirements:

- **Resolution:** The ability to resolve fine details is an important feature of the optical system.
- **Wavelength Range:** Optical devices may be required to operate throughout a given wavelength range, particularly in applications having several sources of light.
- **Environmental Conditions:** Optical systems intended for harsh conditions like severe temperatures or high levels of humidity must be able to resist these circumstances without sacrificing performance.
- **Alignment Tolerance:** Alignment tolerances should be considered while designing optical systems, allowing for simplicity of integration and alignment during production and installation.

1.5 Eastern Anatolia Observatory (DAG)

The DAG telescope at the East Anatolian Observatory is a 4-m class telescope dedicated to working in the visible and near-infrared spectral regions [1]. The telescope will be equipped with Adaptive Optics (AO) system to improve observation conditions with higher resolutions by compensating for the distortion that occurred in the atmosphere [21]. Large-diameter mirrors usually have an Active Optics (aO) system. This technology is employed to actively shape the mirrors in order to prevent certain deformations caused by external disturbances to the optical wavefronts, such as wind,

Table 1.2: Optical Design of the DAG Telescope [1]

DAG Telescope Optical Specifications	
Design Type	Ritchey-Chrétien Telescope
Primary Mirror (M1)	Concave Hyperbolic
Secondary Mirror (M2)	Convex Hyperbolic
Tertiary Mirror (M3)	Flat and Rotational
Focus Type	Two Nasmyth Foci (N1, N2)
Entrance Pupil	3940 mm
Focal Length	56000 mm
Telescope's F-number	f/14.2
Image Space Numerical Aperture	0.03515684
Field of View (Seeing-limit)	24 arcmin
Field of View (Diffraction-limit)	7 arcmin
Plate Scale	3.7 arcsec/mm

temperature, and mechanical stress [22]. In Table 1.2, the optical parameters of the DAG telescope are introduced and the optical layout is shown in Figure 1.2.

The DAG telescope consists of a concave hyperbolic mirror of 4-m class as a primary mirror, followed by a convex hyperbolic mirror as a secondary mirror. It is based on Ritchey-Chretien optical design with an azimuthal mount and a tertiary flat mirror guiding the light to two Nasmyth foci, N1 and N2. In this design, all the mirrors have an active compensation with 66 actuators only at the primary one. The telescope's wide field of view is 24 arcminutes and the F-number at its focal plane is F/14.2 with a plate scale value of 3.7 arcsec/mm [23]. The observatory is located at Karakaya summit in the city of Erzurum, where the seeing limit was measured to be $0.9''$ [24].

1.5.1 Focal Plane Instrumentation (FPI) for DAG

The focal plane instrumentation project is meant to develop imaging and spectroscopic scientific instruments that will be added to the DAG telescope. Part of this

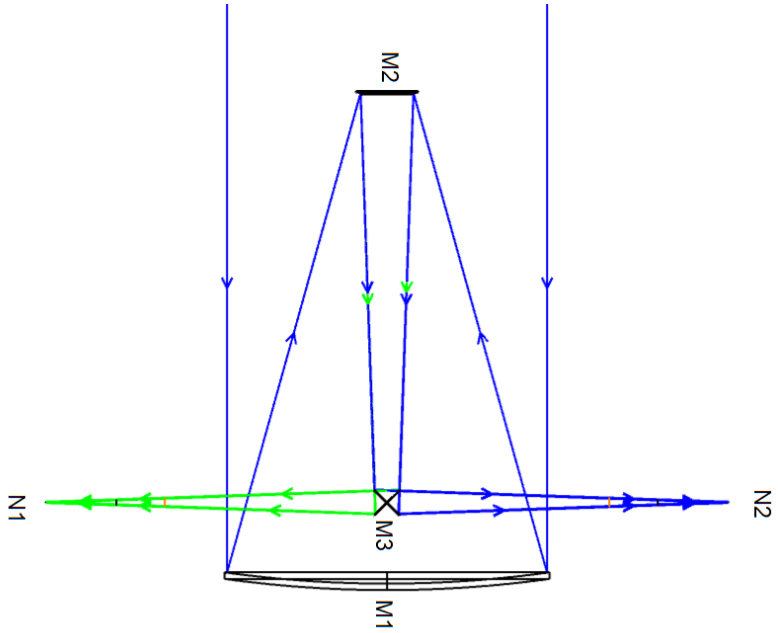


Figure 1.2: Layout for the Optics of the DAG Telescope with Two Nasmyth Foci

project includes measurement, testing and calibration of these novel instruments. FPI is a scientific project funded by the Turkish Ministry of Development [25].

1.6 Objectives of this work and Its organization

The main objective of this study is to design an integral field unit that produces the spectrum of the largest possible areas of the sky with the highest possible optical throughput at the intermediate spectral resolution range. A high optical throughput and a design with high manufacturability are desired. A volume-phase holographic (VPH) grating-based spectrograph achieves high diffraction efficiency in a moderate spectral resolution range which meets the requirements for high optical throughput. An integral field unit (IFU) is designed with its fore-optics in order to carry the most possible spatial extent to the entrance of the spectrograph.

In this chapter, a short introduction to astronomical instrumentation was given, followed by an explanation of the DAG observatory and its capabilities. In chapter 2,

the methodology behind the optical design of the IFU-based spectrograph will be explained thoroughly, with an extensive explanation of the optical design and photonics design processes. In chapter 3, the results of designing several integral field units by utilizing telecentric magnifier lenses with a fiber array directly were discussed, and then a hexagonal microLens array was designed, as well as the optical performance of both methods. In chapter 4, the results of optimizing the parameters of the Volume-Phase Holographic grating using rigorous-coupled wave analysis RCWA was shown for several wavelength ranges. In chapter 5, the optical design of the spectrograph with all optical performance metrics and analysis were illustrated. Chapter 6 is intended to conclude this thesis' work.

CHAPTER 2

METHODOLOGY

Astronomical observatories are going through massive advancements in the last two decades. They have high-resolution imagers and spectrographs. From ground-based telescopes to space ones, scientists are working hard to acquire a better understanding of our universe. Consequently, this has led to pushing the limits of the current state-of-the-art. In that regard, astronomical instruments are gradually being massively complex, making the designer's job more complicated. Due to the increasing number of components in each instrument, the design process has to include integration and coordination between each subsystem so that each part works smoothly together. For example, for an optical designer to work on such a system has to communicate the scientific needs and technical requirements of the astronomical instrument with several partners. This starts by studying the observatory's limits to negotiate further the instrument's requirements with scientists, engineers and technicians. In short, astronomical instrumentation has been a field where many disciplines meet.

In this chapter, the methodology required in the design process of a spectrograph will be discussed. To start with, the technical requirements and scientific needs will be defined. Then, the methods used in calculating the optimum parameter for each subsystem, according to the big picture that will be drawn for the spectrograph, will be introduced.

2.1 Spectrograph Design

Spectrographs, including resolving capabilities, structural differences and optical design, could be classified differently. Several types of spectrographs are based on the

design and operating principles. The spectrograph's type can be defined based on the optical elements used in the design. For instance, using total reflective optics of mirror collimator, mirror camera and reflective grating, the final design is called Czerny-Turner spectrometer [26]. On the other hand, if a combination of reflective and refractive optics is used, the final design is called a catadioptric spectrograph.

There are other types such as prism spectrographs, grating spectrographs, Echelle spectrographs based on the cross-dispersion working principle and Fourier Transform spectrographs. Moreover, the most popular classification is according to their resolving capabilities. There are three types of spectrographs.

- **Low-Resolution Spectrograph**
  The spectral resolution R in that class is less than 1000. It provides an overview of the spectrum without showing resolving fine details. They are usually used for astronomical surveys and explorers.

- **Medium-Resolution Spectrograph**
  The spectral resolution R in that class is from 1,000 to 10,000. Thus, moderate level of spectral resolution is suitable for capturing important spectral details while keeping the signal-to-noise ratio (SNR) at a reasonable level. This balance between spectral resolution and SNR is important in some observation conditions.

- **High-resolution spectrograph**
  The spectral resolution R in that class ranges from 10,000 to 100,000. This spectral resolution range enables precise measurements of spectral lines and advanced analysis.

The final choice of resolution depends on the specific application and the scientific needs. Even if the high-spectral-resolution spectrographs provide precise measurements and extensive spectral details, they require longer exposure time, low optical throughput and high signal-to-noise ratios which is unfavorable in some observational cases. This brings the importance of discussing the scientific needs mentioned in Chapter 1.

2.2 Optical Design of a spectrograph

This section represents the design method of each optical element and the required geometrical optics solution to achieve the systems requirements needed to fit the scientific needs. Spectrographs consist of an entrance slit, collimator, disperser, focusing camera optics and a CCD.

2.2.1 Entrance Slit

A spectrograph is used to re-image the entrance slit into the CCD. The optics of the spectrograph can be said to be in the form of a finite-conjugate system where reimaging occurs at the detector space. The dimensions of the entrance's slit size depend on the field of view needed for spectroscopy. For multi-object spectroscopy, the slit may include some masks to block the light from other sources out of interest. The mask's primary purpose is to prevent the cross-talk that may occur at the CCD detector. The image is transferred from the telescope's focal plane to the entrance slit using fibers for integral field spectroscopy using fiber-fed methods. This method comes with the advantage of organizing the entrance slit to fit the fibers in a one-dimensional order such that the CCD plane includes the spatial and spectral content in the two dimensions of the CCD.

2.2.2 Collimation

Light needs to be parallel before hitting the disperser surface. This is to allow different beams to be dispersed in an organized manner. Collimators can be reflective or transmissive. many designs utilize spherical mirrors or off-axis parabolas (OAP) to collimate the light. The spherical mirror causes an obstruction problem, and the OAP is hard to align. The easiest solution is to use lenses with multiple elements to achieve this purpose. Its main drawback is the decrease in the overall optical throughput of the whole system.

2.2.3 Disperser

Disperser elements have great importance in separating light into its constituent wavelengths. They are considered as the core elements in spectrographs, which allow scientists to study and analyze the spectrum of various light sources. Dispersers separate the light by introducing a certain angular separation for each wavelength. There are several types of dispersers commonly used in the field of spectroscopy. These types commonly vary according to their spectral resolving power, optical throughput, wavelength coverage and efficiency. Below, a short introduction to these popular elements is given.

- Prisms.
  The main working principle in prisms is refraction where the separation of colors occurs based on the varying degrees of bending. Although prisms can offer a wide range of wavelength range, the final spectrum usually suffers from chromatic aberration and low dispersion efficiency.

- Gratings.
  The main working principle in gratings is diffraction which occurs when light passes through a certain obstacle. These obstacles are parallel and closely spaced grooves built into the surface of the grating allowing incident light to be reflected or transmitted in different orders with certain wavelength separations. Gratings are widely used in spectrographs as they provide high diffraction efficiency and spectral resolving power. Gratings can be reflective or transmissive. Their grooves can be ruled over the surface or holographically produced over the volume.

- Grisms.
  A grism, as its name suggests, combines a prism and a grating together. They are known for making the optical design of the spectrometer on-axis which allows a high possibility of beam control. In this combination, the resulting negative dispersion made by the grating is canceled with the positive dispersion made by the prism. This allows the spectrograph to be more compact and always straight on-axis designs. Adding the prism also increases the dispersion

efficiency allowing more separation between wavelengths due to light refraction on the prism's surface [27].

- Echelle Gratings.
  In diffraction grating, as diffraction orders increases, resolving power increases too. However, the main drawback is that the light intensity is not high at high orders, and going further in diffraction order less light can be gathered. This increased the importance of concentrating the energy on high orders.

  The French word Echelle (translated as a ladder) gives an idea of how an Echelle grating really looks. The surface of the grating is introduced to a high blazed angle with the grooves. Echelle grating is usually used in cross-dispersion spectrographs where two dispersion stages are made to increase the instrument's overall spectral resolution [28].

2.2.4 Focusing Camera Optics

This is the hardest part of the process of designing the optics of the spectrographs. Once the incident collimated light passes through the disperser, it must be well-imaged at the detector. The purpose of using focusing optics after the disperser is to make the spatial part well-projected on one axis of the CCD and the spectral part well-imaged on the other axis. The main difficulty of this part is that the camera optics is usually dependent on the slit, collimator and disperser's optical parameters. In that sense, it must be designed after several considerations [29]. Last to mention is reducing higher-order aberrations and introducing mechanical tolerances to the design.

2.2.5 Charge-Coupled Devices CCD

Charge-Coupled Devices (CCDs) have revolutionized observational astronomy. CCDs are used in astronomical work of imaging, astrometry, photometry and spectroscopy. Three major advantages of using CCD in astronomy are low-noise performance, increased quantum efficiencies and faster read-out. Beyond their high QE and low noise characteristics, silicon-based CCDs are widely used in spectrographs due to their broad free spectral range spanning from 300 nm to 1100 nm as well as their

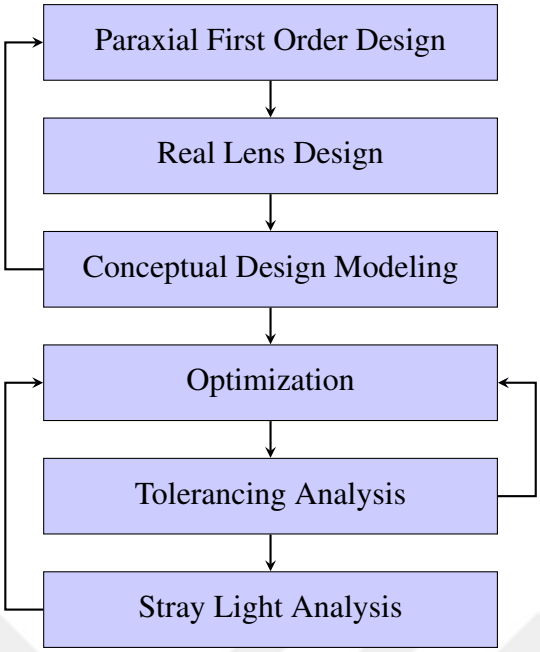


Figure 2.1: The summary of the optical design process of a spectrograph.

large dynamic range which allows the detection of absorption and emission lines and in the same manner continuum radiation. InGaAs-based CCDs extend the spectral range to cover the near-infrared bands, covering the spectral range from 1100 nm up to 1700 nm [30, 31]. Nowadays, CCDs are available in 4k×4k pixel format with a pixel size of 12 microns in the optical band [32].

2.3 Optical Design Process

Optical design starts from first principles and then adds up real-world complexities to the overall system. It starts with the first-order paraxial approximation optics and then moves to thick lenses with glass materials and aberration theories. The optical design process is summarized in Fig. 2.1.

The optical design of a spectrograph based on an integral field spectroscopy follows different design stages. It starts with the consideration of the telescope optics that is meant to be added to. The optical design of this type of spectrograph is summarized in Fig. 2.2.

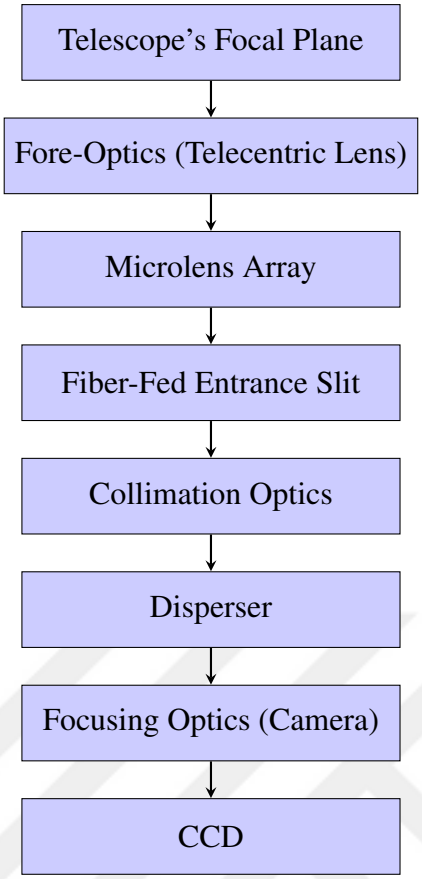


Figure 2.2: The summary of the optical design process involving an integral field spectrograph.

2.3.1 The First Order Optical Design

In the first-order optical design, the light beams traveling through the optical system are assumed to make small angles with the optical axis of the system which allows to utilise linear approximations rather than trigonometric ones. This is known as para-axial approximation. The para-axial approximation is a quick and straightforward technique. It assists the designer how each part interacts with the light rays entering the system and therefore comprehend the size of the design.

2.3.1.1 Thin lens

A thin lens is an essential element in first-order optical design process. The thickness of a thin lens is ideally zero. The nodal points and the principal planes of thin lens are located at the lens. The equation that governs how thin lenses interact with light rays is called the 'lens maker equation' and it is derived by utilising Snell's law. Snell's law describes how light is refracted when passing between two media with different indices of refraction:

$$n_1 \sin(\theta_1) = n_2 \sin(\theta_2) \tag{2.1}$$

where n_1 and n_2 are indices of refraction of the media, θ_1 is the angle the incident ray makes with the surface normal and θ_2 is the angle the refracted ray makes with the surface normal. The equivalent form of thin lens equation is given as

$$\frac{1}{f} = \frac{1}{s_i} + \frac{1}{s_o} \tag{2.2}$$

where s_o is the distance of the object to the lens, s_i is the distance of the image from the lens. Thin lenses are essential building blocks of first order optics that are frequently utilised for controlling light beams, focusing pictures and creating magnification effects.

2.3.1.2 Thick Lenses

In using thick lenses, rules of geometrical optics are still valid but real lenses made up of thick glasses are used. The following concepts are introduced in the design: Refractive index, principal planes, calculation of the effective focal length, front focal length, back focal length, central and edge thicknesses and radius of curvatures. Unlike thin lenses, the thickness of a thick lens cannot be neglected. In thick lens analysis one has to take into account an extra assumption that light ray bends inside the lens and bends at both ends of the lens. Using Snell's law and assuming that the lens is placed in air (n_1=1), lens maker equation is written as

$$\frac{1}{f} = (n-1)\left[\frac{1}{R_1} - \frac{1}{R_2} + \frac{(n-1)\times d}{n \times R_1 \times R_2}\right] \tag{2.3}$$

where R_1 and R_2 are the radii of curvature of the lens, f is the focal length of the lens and d is the thickness. Since the thickness is zero the final form of the equation is:

$$\frac{1}{f} = (n-1)\left[\frac{1}{R_1} - \frac{1}{R_2}\right] \tag{2.4}$$

2.3.2 Lagrange Invariant

Lagrange invariant is a constant for the cone of light that propagates through an optical system. This optical invariant is formed by understanding the ray height and angles of two rays: the marginal and chief rays. It is invariant for refraction and transfer in mediums. For a finite-conjugate imaging system, there is a proportionality constant known by the optical invariant between the height (chief ray height) and the subtended angle (marginal ray angle) and the refractive index of the medium the rays are moving through. The formulation of the Lagrange invariant (H) can be understood by the propagation of the paraxial marginal and chief rays:

$$\mathrm{H} = n\bar{u}y - nu\bar{y} \tag{2.5}$$

2.3.3 Optical Throughput AΩ

The optical throughput is the capacity of an optical system to transfer optical power or flux (for a schematic layout see upper panel of Fig. 2.3). It is expressed mathematically as the AΩ product. A is the pupil area and Ω is the solid angle subtended at this pupil by the object or image. The AΩ is proportional to the square of the Lagrange invariant. The optical throughput is a critical quantity for celestial faint objects detection[33]. Optical throughput can also be called 'etendue' where it gives an idea about how the optical system transmits light after considering losses. Losses can be due to absorption, scattering, alignment and coupling, mismatched polarization and dispersion.

The systems shown in Fig. 2.3 (bottom panel) is useful in finite conjugate systems. Dealing with the optical system as a black box helps the optical designer to deal only with the object and image pupils and their subtended angles while propagating.

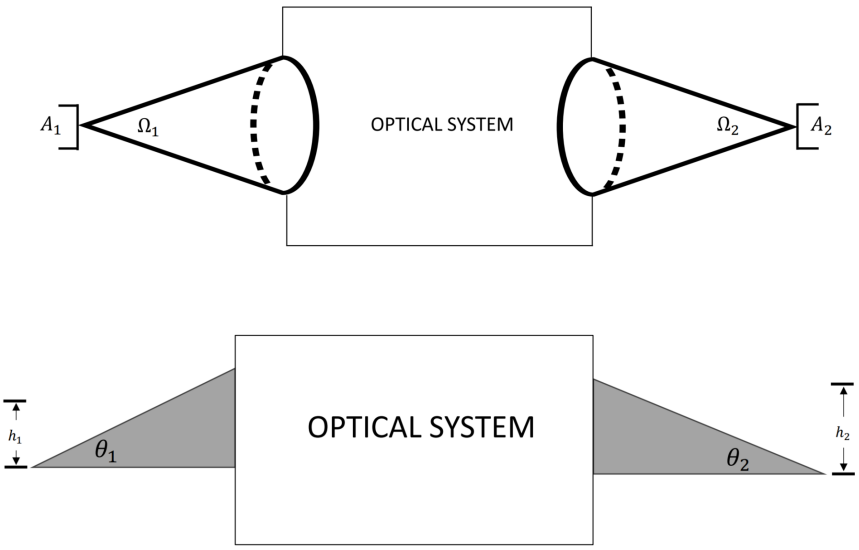


Figure 2.3: (Upper Panel) Optical throughput and cone of rays where A represents the area and Ω represents the solid angle. (Bottom Panel) Optical invariant where h is the chief ray height and θ is the marginal ray angle and the optical invariant for the finite-conjugate systems is equal in both the object and image space as $n_1 h_1 \theta_1 = n_2 h_2 \theta_2$.

2.3.4 Using Optical Design Software for Optimization

OpticStudio (Zemax) is a specialized optical design simulation program used mainly by optical designers. It is used to model the propagation of light through optical systems by geometrical ray tracing and to apply several optimization algorithms in order to improve the design quality with several quality metrics such as MTF, physical optics, aberrations and more [34]. Zemax OpticStudio comes with huge modeling packets for image quality analysis, tolerancing analysis, stray light and many different metrics.

2.4 Geometrical Optics of a Spectrograph

In designing a spectrograph, a basic optical layout is needed to calculate the optics of each part (see Figure 2.4). For example, the designer needs to identify the parameters that will affect the overall performance of the spectrograph for an intermediate

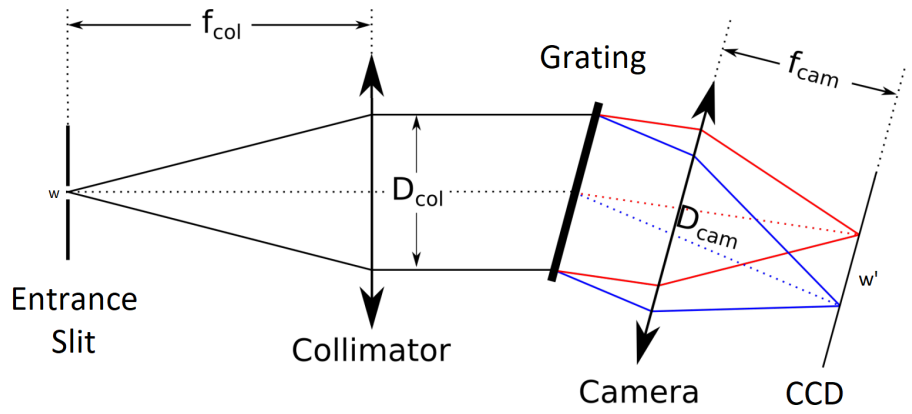


Figure 2.4: Basic Optics of a Spectrograph Based on Thin Lens Paraxial Approximation (Adapted from [2]).

spectral resolution with a diffraction limit near the pixel size for proper sampling. The light enters from the left and follows the following units with their defined parameters: A slit with size w; a collimator of focal length f_{col}, diameter of D_{Col}; a dispersing element (grating) of length L_{grat}, known incidence angle α, diffraction angle β with specific grooves or line density known by spatial frequency v of lines per mm or lpmm (reciprocal of the line density is d); a camera optics (focal length f_{cam}, diameter D_{cam}) to focus the diffracted beams; The CCD camera is in square shape of w' in length with pixel pitch size of μ.

The optical design of this spectrograph is based on Littrow configuration in which the blaze angle is identical to the incidence and diffraction of the grating. In that way, it satisfies $\alpha = \beta = \theta_B$. The diffraction for diffraction grating can be expressed by Bragg's law as

$$m\lambda = d\,(\sin\alpha + \sin\beta) \tag{2.6}$$

After the light passes through the diffraction grating, a variation of angular spread of light per each wavelength occurs. The separation between the angular positions for each wavelength can be expressed by the angular dispersion:

$$A = \frac{d\beta}{d\lambda} = \frac{m}{d\cos\beta} \tag{2.7}$$

Unlike the concept of angular dispersion A which deals with the angular separation of wavelengths, linear dispersion focuses on how the different wavelengths spread out

in space. The linear dispersion can be expressed as

$$\frac{dx}{d\lambda} = Af_{\text{cam}} = \frac{m \cdot f_{\text{cam}}}{d\cos\beta} \tag{2.8}$$

The resolving power which refers to the theoretical value in which the disperser is able to disperse light is given as

$$R = L_{\text{grat}} \cdot v = \frac{L_{\text{grat}}}{d} \tag{2.9}$$

The minimum resolvable spectral size is based on $\Delta\lambda$ which can be thought of as a representation of the smallest difference in wavelength that the spectrograph can distinguish as two separate spectral lines. It can be mathematically expressed by knowing the size of the CCD camera where $dx = w'$ as

$$\Delta\lambda = dx\frac{d\lambda}{dx} = w'\,\frac{d\cdot\cos\beta}{m\cdot f_{\text{cam}}} \tag{2.10}$$

The spectrograph is optically functioning as a re-imager. It reimages the entrance slit (Object-Space) into the CCD camera (Image-Space). The subtended angles in both spaces can be expressed as small paraxial angles in which $d\alpha = w/f_{\text{coll}}$ and $d\beta = w'/f_{\text{cam}}$. Due to Littrow configuration where the incidence angle α is equal to the diffraction angle β, the anamorphic magnification is unity and leads to an equal diameter size of the collimator and the camera optics. In that way, the spectral resolution $\mathcal{R}$ can be expressed by the optics of the object space variables or image space parameters as

$$\mathcal{R} = \frac{\lambda}{\Delta\lambda} = \frac{\lambda}{w'}\frac{mf_{\text{cam}}}{d\cdot\cos\beta} = \frac{\lambda}{w}\frac{mf_{\text{coll}}}{d\cdot\cos\alpha} \tag{2.11}$$

Finally, spectral dispersion per pixel can be expressed as

$$\mu\frac{d\lambda}{dx} = \mu\frac{1}{Af_{\text{cam}}} = \mu\frac{d\cos\beta}{mf_{\text{cam}}} \tag{2.12}$$

2.5 Integral Field Spectroscopy

Integral field Spectroscopy (IFS) is a method that helps astronomers extract the spectrum of the celestial objects of interest with their spatial extent.

In the past, astronomers used a long slit spectrograph to obtain the spectra of extended objects (galaxies or nebula). A long slit was directed to capture sequential spatial

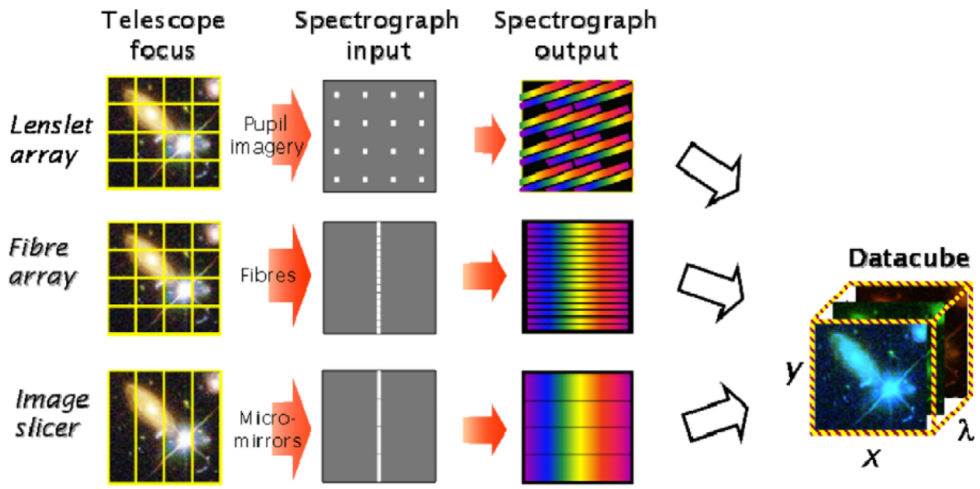


Figure 2.5: Schematic explanation of integral field spectroscopy (adapted from [3]).

segments per each exposure. Then, the process was repeated to cover the whole spatial area. This was a time-consuming and complicated method.

Recently, several techniques have been developed to reduce the exposure time and simultaneously gather as much spatial content as possible. One method is called "three-dimensional spectroscopy". It provides a 3D data cube having a two-dimensional spatial content with a depth of spectral information as the third dimension as seen in Figure 2.5. An integral field unit is a fore-optics system that feeds a spectrograph with sky images with the highest possible throughput. There are three popular methods of achieving this based on the study made by Jeremy Allington-Smith [3].

The main objective in our design for integral field units (IFU) is to correctly transfer the two-dimensional scene at the focal plane of the telescope to a one-dimensional slit of fibers. IFUs use a telecentric magnifying lens followed by a microlens array (MLA) to feed an array of multimode fibers. After the fibers have been properly deployed, a one-dimensional slit is presented at the other end of the fibers. This 1D slit is the entrance aperture of a spectrograph. A two-dimensional microlens array followed by a fiber array is used to divide the field of view into segments. In this way, the fibers act to reconfigure the two-dimensional spatial area of the field into a

one-dimensional slit that feeds a spectrograph with the field segments and acts as an entrance aperture.

Once again, the aim is to achieve two-dimensional spectroscopy to understand spatially large objects in the sky. In this respect, the IFU goes beyond single-slit spectrographs by giving astronomers the advantage of understanding large sky areas. By studying the spatial distribution of many celestial objects, astronomers are able to understand several complex astrophysical phenomena such as the kinematics of stars and galaxies, galaxy mergers, star formation and the dynamics of supermassive black holes at the centers of galaxies. It is even possible to understand the history of the interaction between galaxies and stars by observing the outer shells of these galaxies. All these are advantages of the IFU spectroscopy over the traditional one.

2.6 Fiber-Fed Spectroscopy

A fiber array can divide the designated field of view into small segments and then deploy these segments to the entrance slit of the spectrograph. This is useful in making the spectrograph physically independent from the telescope. Usually, fiber-fed spectrographs are located on a platform beside the telescope which makes them more stable and easy-to-deploy. A fiber by itself cannot fill a two-dimensional area completely for three reasons:

- The fiber edge is circular and circular surfaces will have gaps in between while packing that will lead to a lower filling efficiency and a loss of the spatial information required to be deployed to the spectrograph entrance.

- The fiber core is surrounded by cladding and other mechanical constraints. These circular regions are not actively used and occupy areas in the FOV. It reduces the filling efficiency for the same reasons as above.

- Fibers suffer from focal ratio degradation.

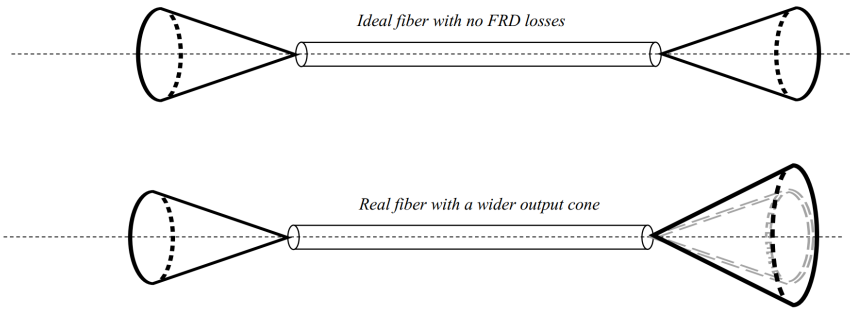


Figure 2.6: Focal ratio degradation and the change in the f-number.

2.6.1 Focal Ratio Degradation (FRD)

FRD refers to the phenomenon that occurs on the optical fibers that causes a degradation in the incident f-ratio, resulting in a faster output f-number (see Figure 2.6). There are two main reasons for this degradation. The first one is a mechanical deformation due to various defects in the fiber such as micro-scale irregularities, localized bending, fiber stress or polishing defects at the fiber end faces [35]. FRD can be represented mathematically as the ratio of the output F-number value to the input F-number value:

$$\mathrm{FRD} = \frac{\mathrm{F_{output}}}{\mathrm{F_{input}}} \tag{2.13}$$

In the ideal case, FRD is unity. Based on the studies done by Barden [4], for most systems having f-numbers below f/5, FRD ratios are found to be close to unity.

As a result, FRD reduces the resolution of spectrographs, distorts the rays received by the spectrograph's CCD camera and adds complexity to the design process of the spectrograph. This can lead to a change in the optical configuration of the spectrograph to be compatible with the subtended angle of the beams propagating from the fibers to the slit of the spectrograph (see Figure 2.7). From the optical designer's point of view, there are two distinct cases. In the best-case scenario, the collimator of the spectrograph will match the output f-number of the fibers very well, and other options will be the worst-case scenario of the designer. As more optical elements are provided to the design, the optics will be more easily adapted to the degradation. However, this might be very difficult to achieve in some other cases.

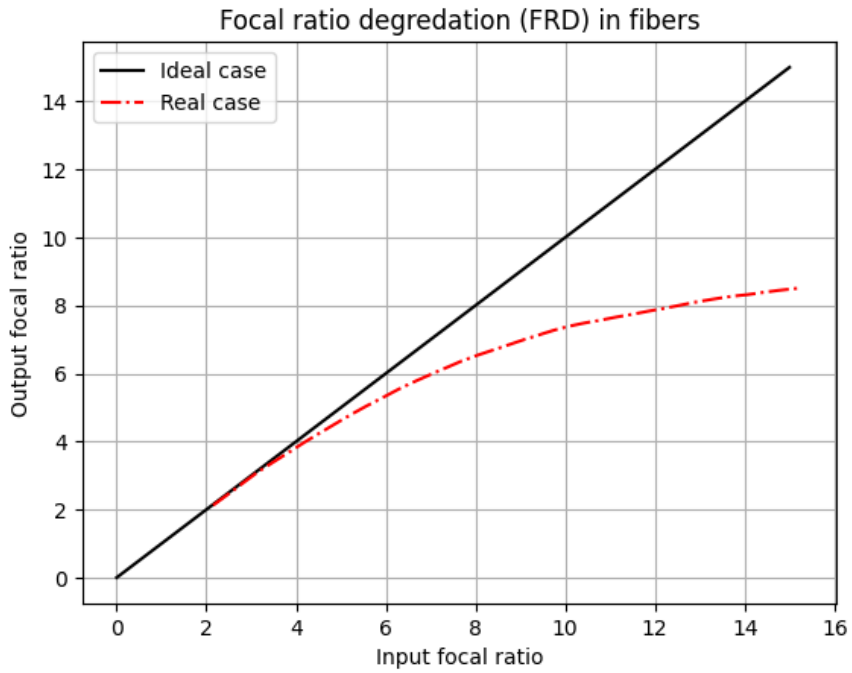


Figure 2.7: Focal ratio degradation and the change in the f-number in real cases (adapted from [4]).

The optical designer should provide a solution to FRD for a spectrograph that is already in use. One solution is to move the collimator lens closer to the fiber output which may result in some reduction in the resolution of the spectroscopic instrument. Another solution is to increase the diameter of the collimator to capture as much of the incoming light as possible. Nonetheless, both solutions have some drawbacks. For example, increasing the size of the collimator requires an increase in the size of other optical components following the collimator (grating, focusing lenses and CCD detectors) which ultimately has an unfavorable effect and, in most cases, is impossible.

2.6.2 IFU using Micro Lens Array (MLA)

Using an array of microlenses to feed the fiber can be thought as “optical magic”. Firstly, by using MLA, all the beams will be focused onto the fiber core which will lead to a dramatic reduction of the effects of the inactive regions around the fiber.

Secondly, the use of MLA allows optical designers to manipulate the cone of rays to minimize the focal ratio reduction by choosing faster f-number.

2.6.3 Multi-Mode Fiber (MMF) Coupling Efficiency

Multi-mode fibers usually make a design of high optical throughput. They have the ability to collect more light compared to single-mode fibers [36]. The coupling efficiency can be mathematically expressed by the AΩ (see section 2.3.3). After passing through a microlens array, the light distribution can be mathematically represented by a point-spread function (PSF) often by a 2D circular Gaussian function. This PSF describes how light is distributed on the image plane. The fiber coupling efficiency quantifies how effectively this modified light is coupled into an optical fiber. After that we can find and measure the diameter of the PSF and whether it is well-fitted into the chosen fiber diameter. This is how we calculate the coupling efficiency.

2.6.4 Fore-Optics for Telecentric Magnification

There are some advantages in magnifying images at the focal plane of a telescope before reaching the microlens array.

- Using MLA with a favorite size. This may allow the designer to use commercial-off-the-shelf (COTS) lenses and reduce the manufacturing costs of the IFU.
- Making the system independent from the telescope. This may include changing the f-number and reducing the FRD too which makes the system independent of the telescope.

The magnified image must be telecentric at the MLA plane. This can be done during the design stage by ensuring the image pupil position is at infinity.

2.6.5 Optical Design of a Telecentric Magnifier

Using ZEMAX, it is possible to design a telecentric magnifier by ensuring the angular magnification is unity during the first-order paraxial design. By using a two-lens

paraxial system, one can magnify or demagnify the image with respect to the object plane and, at the same time, keep the angular magnification at unity. This can be done using two lenses f_a and f_b where the transverse magnification (m_{mag}) required is equal to the ratio of focal lengths:

$$m_{\text{mag}} = \frac{f_b}{f_a} \tag{2.14}$$

This can also be achieved by using the Merit Function optimization operand `PMAG` in Zemax.

Optical telecentric systems have an angular magnification equal to unity. The main goal of the design is to optimize the optics so that the system has a unity angular magnification i.e. $M_\theta = \theta_{\text{i}}/\theta_{\text{o}}$ where θ_{i} is the cone of rays subtended by an angle at the image space and θ_{o} is the cone of rays subtended by an angle at the object space. Therefore, the angular magnification can be kept at unity in paraxial design by using the optimization operand `AMAG` during any optimization condition. For real optics cases, the designer might have three different ways to reserve the telecentrity of the design by doing the following:

1. Use the `EXPP` operand to keep the position of the exit pupil at infinity. This can be done by retrieving the position of the exit pupil using the operand `EXPP` and then taking the reciprocal of it by using the operand `RECI` and making it equal to zero during the optimization.

2. Use chief ray angle to solve for the last surface of the lens f_b and keep the angle equal to zero.

3. Use `RANG` operand to keep the chief angle to zero.

2.6.6 Losses due to Non-Telecentricity

In ideal telecentric cases, the exit pupil is at infinity which introduce no shift in the pupil position. It means that the center of the pupil image is on the optical axis of the microlens. In non-telecentric cases, there is a pupil shift introduced that leads to a shift, as seen in Figure 2.8. The more we get off the optical axis, the higher the introduced shift is. This will eventually reduce the coupling efficiency of the light

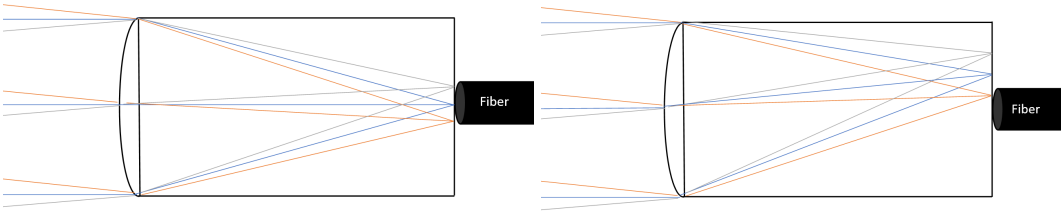


Figure 2.8: Light propagation through a single microlens and the effect of telecentricity on the coupling efficiency

into the fiber and cause a light loss. The relationship between the non-telecentric ray angle and the shift in pupil image can be expressed as the following:

$$\Delta s = f_{\text{MLA}} \tan\left(\frac{\beta}{m_{\text{mag}}}\right) \tag{2.15}$$

where β is the non-telecentric angle at the focal plane of the telescope and f_{MLA} is the focal length of the microlens.

2.7 Volume-Phase Holographic Grating

When light propagates through an obstacle such as a slit or a small aperture, it diffracts. Diffraction can be expressed as a perturbation of the optical waves. It can be represented by several point sources that interfere along the aperture. A hologram, on the other hand, is a diffraction pattern that has already been recorded. When light passes through it, it produces a specific wavefront which can generate an image at a specific location. VPH is the core element for dispersion in modern instruments due to its high line density, large diameter producibility and excellent diffraction efficiency. There are two types of grating surfaces.

- Surface-Relief diffraction grating
- Volume-Phase Holographic (VPH) Grating

VPH gratings show great potential in replacing classical ruled surface-relief (SR) grating due to the following reasons [4]:

- VPH shows high diffraction efficiencies reaching 100%.
- The polarization effect in VPH gratings is less severe than in SR gratings.
- VPH gratings lack many of the anomalies that are common in ruled SR gratings.
- VPH shows fewer ghosts and scattered light
- VPH diffraction efficiency peak can be tuned to shift according to the desired wavelength.
- VPH can be fabricated to high spatial frequencies up to 6000 lines/mm.
- VPH can be fabricated with high diameters up to 800 mm.
- Due to the fact that the photosensitive material (DCG) is sandwiched between two glass substrates, the VPH can be easily cleaned and has a longer lifetime than ruled SR gratings.
- VPH can be coated with anti-reflection coatings introducing high optical throughput and less portion of light get scattered on the surface.
- VPH can be easily customized
- VPH can be designed to work in Littrow configuration resulting in an easy camera optics design.

The higher the line density in VPH grating, the narrower the wavelength and angular bandwidths. This is considered the main drawback of VPH grating. Due to this, many VPH-based spectrographs are made of several spectral arms to cover a wider range.

The VPH grating has a sinusoidal modulation of the refractive index over its volume. It produces a phase shift according to the wavelength of the incident beam. According to the phase difference, an interference pattern is produced. The sinusoidal modulation or variation in the refractive index can be mathematically expressed as

$$n(x,z) = n_{\text{DCG}} + \Delta n \cdot \sin\left(2\pi/d \cdot (x\sin\phi + z\cos\phi)\right) \tag{2.16}$$

where n_{DCG} represents the refractive index of the Dichromated Gelatin (DCG) material used in the VPH grating, Δn is the refractive index modulation, d refers to

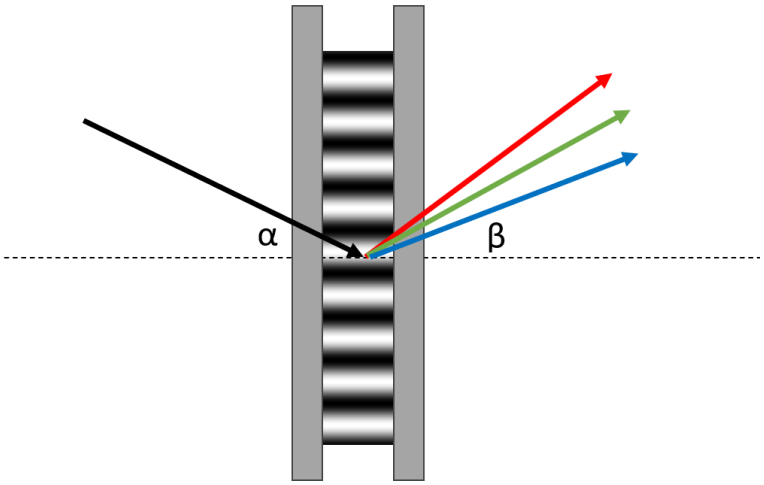


Figure 2.9: Light passing through the VPH surfaces, the width of the DCG is not to scale

the groove spacing of the grating and ϕ denotes the slant angle of the fringes on the grating.

Produced fringes can be parallel to the surface with a slant angle equal to zero. At this point, the diffraction occurs according to the Littrow configuration where the incident angle α is equal to the diffraction angle β (see Figure 2.9).

The Rigorous Coupled-Wave Analysis (RCWA) provides an exact solution and formulation to the diffraction efficiency of the VPH grating [27]. Proper modelling of the VPH grating is essential in calculating the parameters such as the sinusoidal index variation, thickness of the Dichromated-Gelatin film, grooves density and the incidence angle based on the wavelength desired (see Figure 2.10). A robust RCWA is not essential in the optical design phase; instead, a first-order approximation of the RCWA made by Kogelnik's approximation that is accurate (to within 1%) is enough when $Q > 10$ [37].

$$Q = \frac{\lambda^2}{d^2 n_{\text{DCG}} \Delta n} \tag{2.17}$$

where t is the thickness of the DCG material inside the grating and d is the spacing between grooves. The incidence angle for Bragg's condition according to the Littrow

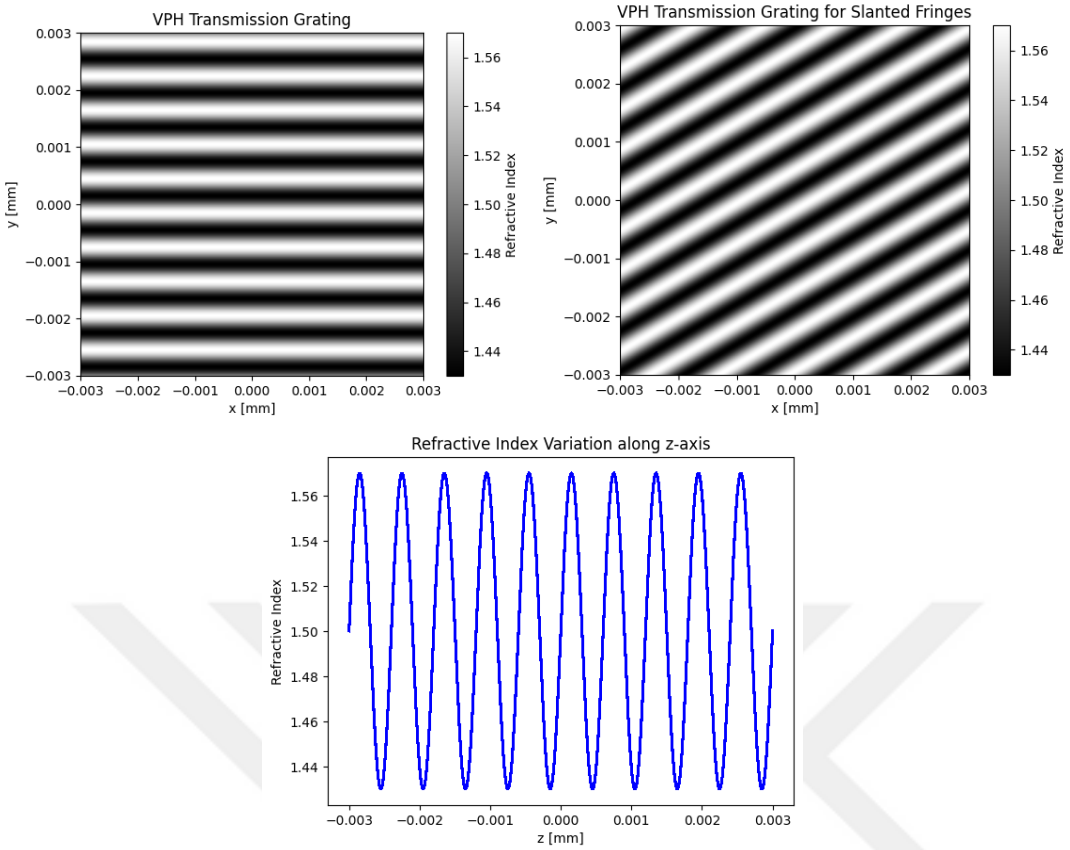


Figure 2.10: Sinusoidal variation of the refractive index according to Littrow Configuration, where the grooves are parallel to the optical axis (top-left panel). The grooves have slanted angle to the optical axis (top-right panel). The depth of variation of the refractive index on the z-axis (bottom panel).

configuration can be expressed as

$$\alpha = \sin^{-1}\left(\frac{\lambda_c v}{2}\right) \tag{2.18}$$

The diffraction efficiency of any unpolarized incident beam can then be calculated using Kogelnik's approximation as the average of the efficiencies in the two polarization directions of efficiencies η_p and η_s as in Equation 2.19.

$$\eta = \frac{\eta_s + \eta_p}{2} = \frac{1}{2}\sin^2\left(\frac{\pi \cdot t \cdot \Delta n}{\lambda_c \cdot \cos\alpha}\right) + \frac{1}{2}\sin^2\left(\frac{\pi \cdot t \cdot \Delta n}{\lambda_c \cdot \cos\alpha} \cdot \cos(2\alpha)\right) \tag{2.19}$$

2.8 Spectrograph Design Consideration

After using Kogelnik's approximation, the desired high spectral resolution could be achieved by using a high number of lines (or groove density). But the higher the groove density, the narrower the FWHM of the diffraction efficiency. This will lead to a narrow spectral coverage of the spectrograph. A solution of having several spectral arms is required in the design by diving the light beam using dichroic mirrors to achieve an overall wider spectral range optical throughput. In our cases, each arm could be designed according to the geometrical optics per each wavelength range and its corresponding diffraction angle:

$$\begin{aligned} m\lambda_1 &= d\left(\sin\alpha + \sin\beta_1\right) \\ m\lambda_2 &= d\left(\sin\alpha + \sin\beta_2\right) \\ \beta_1 &= \arcsin\left(\frac{m\lambda_1}{d}\right) - \sin\alpha \\ \beta_2 &= \arcsin\left(\frac{m\lambda_2}{d}\right) - \sin\alpha \\ d\beta &= \beta_2 - \beta_1 = \frac{w'}{f_{\text{cam}}} \end{aligned} \tag{2.20}$$

CHAPTER 3

INTEGRAL FIELD UNIT (IFU) DESIGN

3.1 Introduction

Integral field units provide a handful interface to deploy images from the telescope's focal plane into the entrance slit of the spectrograph. This method is known as Integral Field Spectroscopy (IFS). The main purpose of this study is to feed the entrance slit of a spectrograph with a narrow 1D fiber array that has a size less than 1 mm. At the same time, the most possible spatial content has to be covered with the highest possible coupling efficiencies. The figures of merit of this design are coupling efficiencies, slit size, spatial content covered and manufacturability.

3.2 First IFU Design using a Fiber Array

Firstly, a mathematical model was used to achieve an optimal grid of circular fibers for complete coverage in a square region (see Figure 3.1). This can be achieved by observing already manufactured multi-mode fibers. In that way, a prior knowledge of commercial fiber parameters could be obtained: Fiber core diameter, fiber cladding size and mechanical spacing in between fibers. The used fiber array specifications for the initial design are given in Table 3.1.

The fiber array is in a square shape of 20 mm by 20 mm. The magnifier at the fore-optics is used to re-image the $30'' \times 30''$ field of view using the plate scale of our telescope. This field of view corresponds to 8.0999872 mm at the telescope's focal plane. The transverse magnification required for a square fiber array can be calculated such that $m = y_o/y_i = 20/8.0999872 = 2.46913$. The magnifier can flip the image

Table 3.1: IFU initial design parameters using a fiber array.

Parameter	Value
Field of View	$30'' \times 30''$
Field of View per fiber	$1.36''$
Fiber Core Diameter (D_{core})	0.9 mm
Fiber Cladding and Spacing	0.923 mm
Array Size	20×20 mm
Number of Fibers	484 fibers
Filling Efficiency	47.509%
Slit Size at the Spectrograph Entrance	446.732 mm

and the value of the transverse/spatial magnification may be given with a negative value.

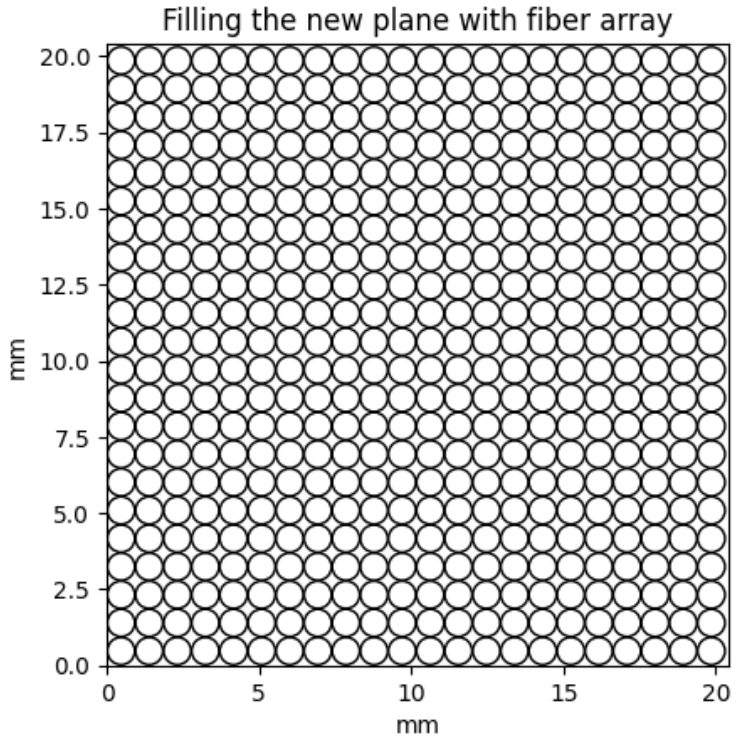


Figure 3.1: Filling the fibers at the magnifier focal plane.

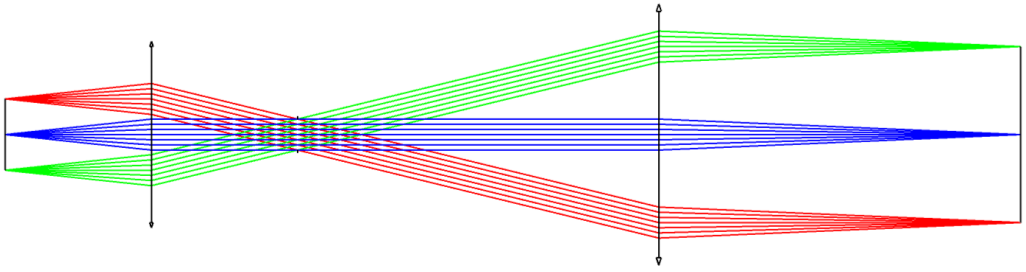


Figure 3.2: First-order magnifier lens for the initial design.

3.2.1 Paraxial Design for a Circular IFU array

The design has progressed from the initial calculation stage into OpticStudio/Zemax evaluation stage by using paraxial lenses shown in Figure 3.2. Thus, the calculated results are used in preparing the merit function which is given as

Paraxial Magnification (PMAG) : -2.46913
Angular Magnification (AMAG) : 1
Total Optical Track (TOTR) : 400 mm

After optimizing the optical system based on telecentricity and magnification, the optical system can be defined as follows. The system contains two lenses with focal lengths f_a=50 mm and f_a=123.46 mm. The effective focal length of the magnifier as a whole was as high as expected with EFFL=13382.3 mm. The optical system was chosen to cover the spectral range from 0.4-1.4 μm. The total track of the optical system followed the constraint to be equal to TOTR=297.0214 mm.

3.2.2 Real Optical Design for the circular IFU fiber array

Moving from the first-order paraxial optics design stage to the thick optics design stage using glass, one of the important parameters to consider is the glass type. The preferable glass should be easy to manufacture and at the same time, it has to have a

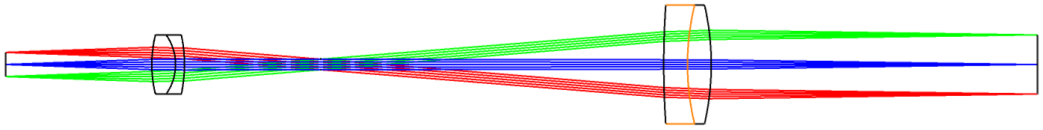


Figure 3.3: Real Optical Design of the Telecentric Magnifier Lens Before the Circular Fiber Array

high transmission ratio. In that regard, while using Zemax's optimizer for choosing optical elements a specific library of optical materials has been chosen to restrict the optimizer to have high transmissive glasses in finalizing the IFU design. The layout of the design is given in Figure 3.3 and lens parameters are listed in Table 3.2.

3.2.3 Optimization for Fiber Coupling Efficiency

In this part, the "Geometric Image Analysis" tool on OpticStudio/Zemax has been utilized to compute multi-mode fiber coupling efficiency. After that, a new operand has been added to the merit function to achieve the highest possible coupling efficiency to this design. The calculation was made to fit into the multi-mode fiber specifications

Table 3.2: Magnifier lens surface data.

Surface	Radius of Curvature (mm)	Thickness (mm)	Glass Code
1	∞	49.18	
2	41.20	8.000	N-BAK1
3	-17.23	3.000	N-KZFS8
4	-47.13	45.90	
5	∞	115.5	
6	293.3	7.999	SF1
7	84.86	8.000	N-PSK53A
8	-89.27	109.8	

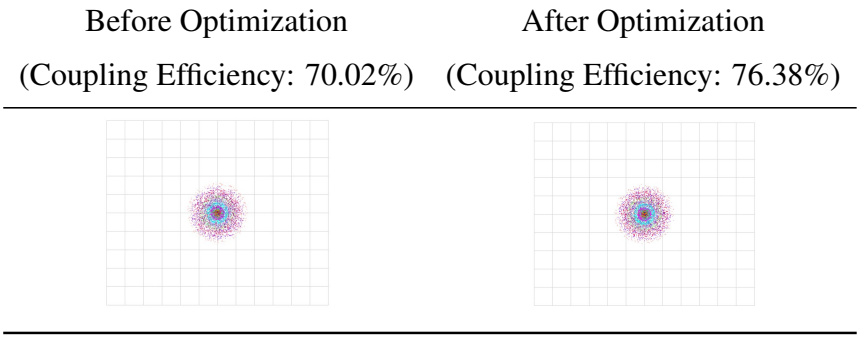


Figure 3.4: Results of optimization for multi-mode coupling efficiency.

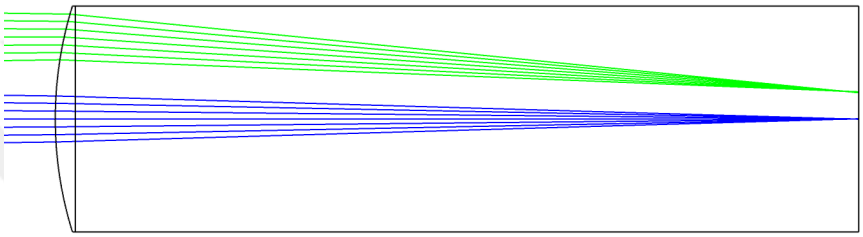


Figure 3.5: Light passing through a single microlens

chosen before filling the array with circular fiber (see previous Table 3.1).

The starting coupling efficiency was 70.02%. After running the optimizer with operand `IMAE` coupling efficiency of 76.83% was reached. This value includes AR coating added to surfaces, and polarization effect was switched on. The spot diagram before and after the optimization are given in Figure 3.4.

3.3 IFU Design using MicroLens Array (MLA)

In the previous stage, efficiency of packing the square area with circular fibers after the magnification was low. To increase the packing efficiency, a hexagonal microlens array has been used on the focal plane at the telecentric magnifier which reaches up to 99% filling efficiency. In this way, the spatial information of the observed object is

Table 3.3: Results of filling the focal plane with a hexagonal grid.

Parameter	Value
Rectangle width	19.44 mm
Rectangle height	20.00 mm
Hexagon side	1.43177 mm
Filling Efficiency	98.63%
Number of Hexagons	60

not lost as in the initial case. The response of a single microlens is shown in Figure 3.5.

In the first attempt to achieve a high fill factor, the same square size (20 mm) was used. On the other hand, a hexagonal grid fits better when one side of the focal plane becomes shorter which is the reason why this design will have different field of views in both horizontal and vertical axes. A Python code was developed to find the best method of filling the area with hexagons. The results of the filling efficiency are listed in Table 3.3 and physical filling is shown in Figure 3.6.

3.3.1 Geometrical Optics Calculations

Based on the geometrical optics of thin and thick lenses (see Section 2.3.1), each of the microlens array is considered a plano-convex lens. The second face of the lens is flat which means that the radius of curvature is at infinity. The most important part of this design is to have the f-number of the MLA to be less than f/4. This is to prevent the focal ratio degradation effect. As a rule of thumb, the f-number is to be chosen as f/3.4. Note that at this f-number the FRD is close to unity and helps to find an easy collimation solution at the spectrograph side too. As seen in the hexagonal grid, the grid almost fills the rectangular side of 20 mm with 8 hexagons. The diameter of a single MLA can be chosen to be D_{MLA} = 20 mm / 8 = 2.5 mm. Since the final f-number was already set, the focal length of each MLA can be obtained:

$$f_{\mathrm{MLA}} = f/\# \times D_{\mathrm{MLA}} \tag{3.1}$$

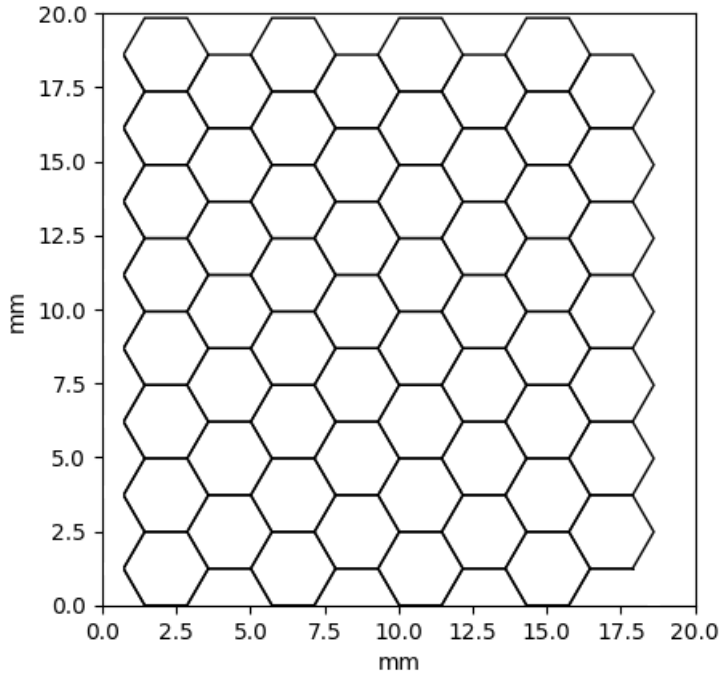


Figure 3.6: Physical look of filling the focal plane with a hexagonal grid.

From the thick lens equation, the plano-convex lens can be solved. The radius of curvature can be calculated as

$$f_{\text{MLA}} = \frac{R}{n(\lambda) - 1} \tag{3.2}$$

At this stage, we choose a high transmissive glass and preferable manufacturers. Under these two criteria, we chose fused silica (fused quartz) with a refractive index of $n = 1.4623$ at $\lambda = 500$ nm (central wavelength of the design). Using [38], the unit hat height of the MLA can be calculated as

$$h = R - \sqrt{R^2 - \frac{D_{\text{MLA}}^2}{4}} \tag{3.3}$$

The final results of the design are shown in Table 3.4.

For any finite conjugate optical system, the Lagrange invariant can be utilized to understand how the light will propagate from the telecentric lens to the microlens array and then to the fibers. In that sense, the product of $nh\theta$ is constant along the

Table 3.4: Microlens Array Design

Parameter	Value
Material	Fused Silica
Wavelength Range (λ)	0.4-1.4 μm
Grid Shape	Hexagonal
Array Type	Rectangular (7×7)
Lens-Type	Plano-convex
Lenslet Pitch (D_{MLA})	2.5 mm
Lenslet Radius (R)	3.91 mm
Lenslet Height (h)	205 μm
Lenslet Depth Thickness (D_{depth})	8.5 mm
Focal Length	8.5 mm
F-Number	f/3.4
AR Coating	Yes

optical path. This concept is used heavily in understanding the light beam passing from each conjugate point such as the telecentric magnifier image plane to the fiber entrance:

$$h_{\text{MAG}}\theta_{\text{MAG}} = n_{\text{silica}}h_{\text{fiber}}\theta_{\text{fiber}} \tag{3.4}$$

where h_{fiber} is the fiber height where in this case it is the fiber core diameter, θ_{fiber} is the subtended angle of rays entering the fiber which has been fixed before when the f-number is also fixed with f/3.4, h_{MAG} is the magnifier lens focal plane height.

At this point, we will choose a similar design based on the initial one (see Figure 3.3). Three variables in Equation 3.4 are known, therefore, we can calculate for θ_{MAG} to modify the initial design according to the new inputs. The transverse magnification at the telecentric magnifier is chosen in the initial design to be equal to 2.46913 and the transverse magnification of the microlens array is the diameter of a single MLA over the fiber core diameter. Therefore,

$$m_{\text{MLA}} = \frac{D_{\text{fiber}}}{D_{\text{MLA}}} = \frac{0.1}{2.5} = 0.04 \tag{3.5}$$

Table 3.5: The hexagonal IFU design parameters.

Parameter	Value
Diagonal FoV	$33.4''$
Effective Focal Length	-13301.35 mm
Total Track	294.7621 mm
Image Space (f/#)	3.4
Image Space NA	0.01424808
Wavelength Range	0.35-1.4 μm
Fiber Number	61
Fiber Core Diameter	100 μm

3.3.2 Design Optimization

As the optical system is circular, the optical diameter is usually chosen to cover the whole image rectangle or square shape. This is usually called the image circle diameter. At this point, after optimization, the field points must be correctly entered into the field grid on ZEMAX such that the image circle shall cover the rectangle of the whole MLA array. The circle surrounding this rectangle has a diameter of 27.87 mm.

A user-defined `us_array_hex.dll` surface on ZEMAX has been used for hexagonal packing. It has provided a different method of distributing the hexagonal grid. The side of each hexagon was kept similar to values given in Table 3.3. The largest diameter of each hexagon (D_{HEX}=2.86 mm) was taken as a reference in calculating the image of the FoV seen by each microlens ($\mathrm{FoV}_{\mathrm{MLA}}$=1.1583 mm) in order to calculate the coupling efficiency. The method of packing has produced the chosen grid to have 61 microlens which leads to 61 fiber arrays. The resulting values of optimized IFU design and surface data are given in Tables 3.5 and 3.6, respectively.

3.4 IFU Final Design

OpticStudio/ZEMAX has a distinctive way of hexagonal packing. It packs these hexagons inside a new hexagon which will result in a filling efficiency close to 100%

Table 3.6: Surface table of the hexagonal IFU design.

Surf	Type	Radius	Thickness	Glass	Clear Diameter
OBJ	STANDARD	∞	49.9749		11.29
1	STANDARD	35.8486	8.0002	N-BAK4HT	20
2	STANDARD	-13.2120	7.4228	F5	20
3	STANDARD	-79.4502	42.8006		20
STO	STANDARD	∞	116.2722		3.52
5	STANDARD	187.9276	7.6819	SF1	30
6	STANDARD	69.5357	7.9150	AF32ECO	30
7	STANDARD	-69.6563	99.5828		30
8	USER DEFINED	3.9100	0.2050	SILICA	7.66
9	STANDARD	∞	8.5000	SILICA	7.66
IMA	STANDARD	∞		SILICA	0.05

Table 3.7: Final results of the IFU design.

Parameter	Value
Diagonal FoV	22.8 arcsec
Single MLA FoV	2.53 arcsec
Fiber Number	61
MLA diameter	2.5 mm
Packing Method	Hexagonal
Aperture Geometry	Hexagon UDA
UDA Scale	0.077
Exit f-number	f/3.4
Fiber Core Diameter	100 μm

as shown in Figure 3.7. In that regard, the user-defined `us_array_hex` surface was used. A different user-defined outer aperture has been chosen from `hexagon.uda` which is another user aperture with a User-Defined Aperture (UDA) of UDA scale of 0.077 in OpticStudio/ZEMAX.

The final results and the final parameters of the IFU design are listed in Tables 3.7

Table 3.8: Final parameters of the IFU design.

Parameter	Value
Single MLA Diameter	50 μm
Fiber Core Diameter	10 μm
Spectrograph Entrance Slit Size	610 μm
Number of Fibers	61
MLA Array Diameter	387.3 μm
Seeing Limit Diameter (Telescope)	243.24 μm
Magnification m	0.20556
Total FoV (Focal Plane)	1.884 mm
IFU Diagonal FoV	6.97″
Focal Length f_a	100 mm
Focal Length f_b	20.556 mm

and 3.8, respectively.

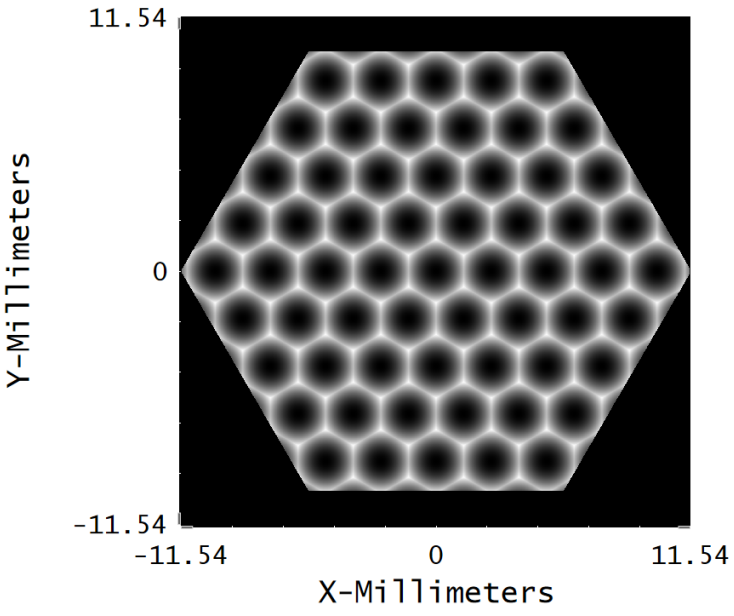


Figure 3.7: Final surface sage of hexagonal lens array with hexagonal packing using Zemax.

CHAPTER 4

PHOTONIC DESIGN OF THE VOLUME-PHASE HOLOGRAPHIC GRATING

The light-matter interaction is the scientific discipline of photonics. The process of designing optical systems and devices to manipulate photons is called photonic design. The main objective of photonic design is to efficiently control and guide photons of light to perform specific functions.

In this chapter, the main purpose is to find the best parameters of materials to guide the light that passes through a diffraction grating in order to have the highest possible transmission spectrum at a specific diffraction order.

For the volume-phase holographic (VPH) grating case, designers used to make RCWA calculations to maximize the first-order diffraction efficiency. The diffraction efficiency can be calculated using equation 2.19. In this mathematical formulation, the diffraction efficiency is the ratio in the intensity of light at the desired diffraction order over the intensity of the incident light. The diffraction order in the case of VPH grating is the first order.

By applying Kogelnik's approximation for the RCWA calculation and developing an optimization code that finds the optimum grating parameters, the highest efficiency will be produced with the widest possible FWHM wavelength range. The code has assumed that the configuration of usage is Littrow and it is under Bragg's condition of superblazed VPH.

The design of modern spectrographs using VPH grating has allowed a high optical throughput due to its high diffraction efficiency. To increase the wavelength range of the design, a three-arm spectrograph was chosen (see Table 4.1). The chosen central

Table 4.1: Optical Requirements for a Three-arm Spectrograph

Arm	$\Delta\lambda$	λ_c	Grating Type	Aim
Blue	400 - 600 nm	~486.135 nm	VPH	H_β
Red	600 - 900 nm	~656.279 nm	VPH	H_α
NIR	1.1 - 1.4 μm	~1.25 μm	VPH	Johnson-K

wavelengths of blue and red arms are aligned with the Balmer's spectral lines of H_β and H_α, respectively In the near-infrared arm, a spectral range in the J-band was selected for its scientific importance in astronomy.

4.1 Blue Arm Design

This arm is intended to work in the blue spectral region and at the peak of the diffraction efficiency to be its central wavelength at the H_β spectral line wavelength. The optimum wavelength was chosen to cover the spectral regions from 400 to 600 nm. Several restrictions were considered to make the grating manufacturable according to the current technologies.

Optimization in the sinusoidal refractive index modulation was run to find the optimum sinusoidal variation in index. The optimum value for the blue arm was found at $\Delta n = 0.096$. This can be seen in Figure 4.1 (top-left).

Another optimization is in the thickness of the VPH grating was run to find the ideal thickness that leads to the highest diffraction efficiency at the central wavelength. The optimum value of the grating's thickness was at t= 6.2 μm. The optimization results can be seen in Figure 4.1 (top-right).

The final diffraction efficiency results are shown at Figure 4.1 (bottom) which considered the transmission spectrum of the chosen diffraction grating. The optimization final results for finding the optimum parameters of VPH diffraction grating at the Bragg Superblaze case are shown in Table 4.2.

Table 4.2: VPH Final Parameters for the Blue Arm. λ_c: Central Wavelength; $\Delta\lambda$: Wavelength Range; ν: Spatial Frequency; t: Grating Thickness; Δn: Sinusoidal Modulation; α: Blaze Angle.

λ_c (nm)	$\Delta\lambda$ (nm)	ν (lines/mm)	t (μm)	Δn	α (°)
486.135	$420 - 550$	2380	6.200	0.096	35.35

4.2 Red Arm Design

This arm is intended to work in the red spectral region and at the peak of the diffraction efficiency to be its central wavelength at the H_α spectral line wavelength. The

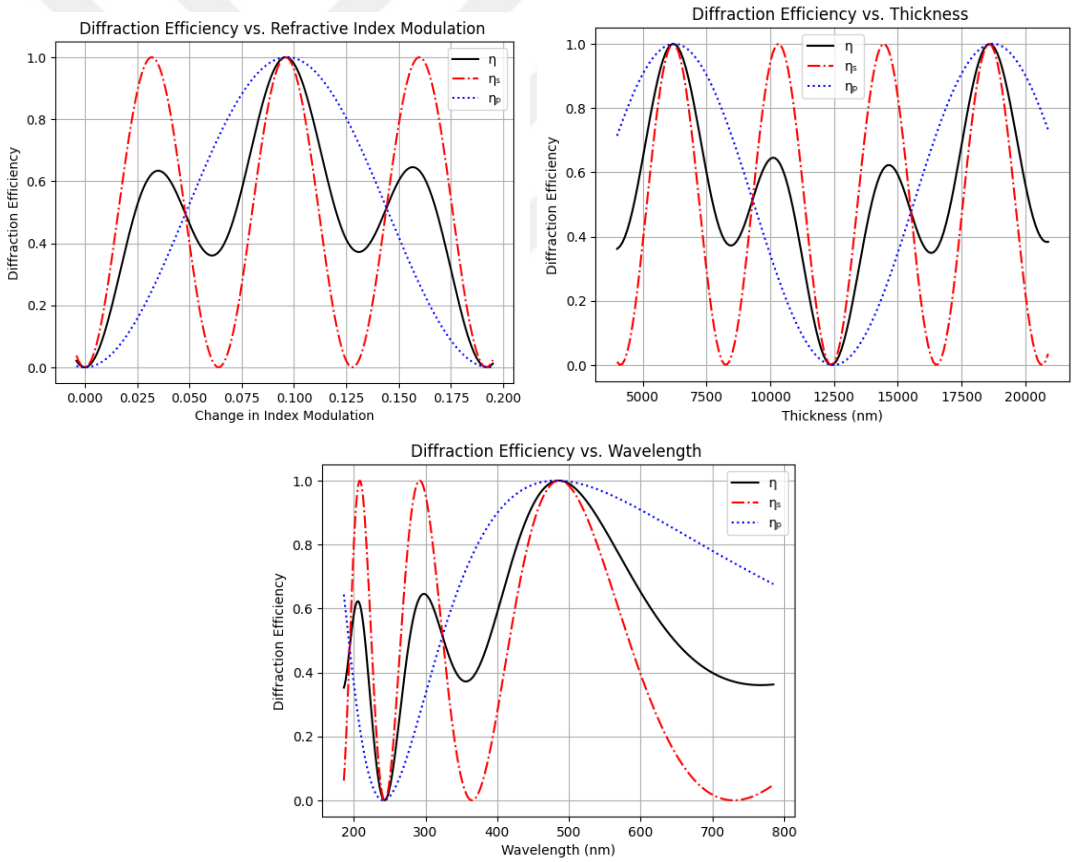


Figure 4.1: Blue Arm diffraction efficiency: (top-left panel) With respect to the sinusoidal refractive index. (top-right panel) With respect to the grating thickness. (bottom panel) With respect to the wavelength.

Table 4.3: VPH Final Parameters for the Red Arm. λ_c: Central Wavelength; $\Delta\lambda$: Wavelength Range; ν: Spatial Frequency; t: Grating Thickness; Δn: Sinusoidal Modulation; α: Blaze Angle.

λ_c (nm)	$\Delta\lambda$ (nm)	ν (lines/mm)	t (μm)	Δn	α (°)
656.279	$550 - 820$	1760	14.1	0.057	35.28

optimum wavelength was chosen to cover the spectral regions from 600 to 900 nm. Several restrictions were considered to make the grating manufacturable according to the current technologies.

Optimization in the sinusoidal refractive index modulation was run to find the optimum sinusoidal variation in index. The optimum value for the blue arm was found at $\Delta n = 0.057$. This can be seen in Figure 4.2 (top-right).

Another optimization in the thickness of the VPH grating was run to find the ideal thickness that leads to the highest diffraction efficiency at the central wavelength. The optimum value of the grating's thickness was at t = 14.1 μm. The optimization results can be seen in Figure 4.2 (top-left).

The final diffraction efficiency results are shown in Figure 4.2 (bottom) which is considered the transmission spectrum of the chosen diffraction grating. The optimization final results for finding the optimum parameters of VPH diffraction grating at the Bragg Superblaze case are shown in Table 4.3.

4.3 Near-Infrared (NIR) Arm Design

This arm is intended to work in the red spectral region and at the peak of the diffraction efficiency to be its central wavelength at the λ_c = 1.25 μm. The optimum wavelength was chosen to cover the spectral regions from 1100 to 1400 nm in the J-band of the near-infrared spectral region. Several restrictions were considered to make the grating manufacturable according to the current technologies.

Optimization in the sinusoidal refractive index modulation was run to find the opti-

mum sinusoidal variation in the index. The optimum value for the NIR arm was found at $\Delta n = 0.099$. This can be seen in Figure 4.3 (top-left).

Another optimization in the thickness of the VPH grating was run to find the ideal thickness that leads to the highest diffraction efficiency at the central wavelength. The optimum value of the grating's thickness was at t=19.900 μm. The optimization results can be seen in Figure 4.3 (top-right).

The final diffraction efficiency results are shown in Figure 4.3 (bottom) which is considered the transmission spectrum of the chosen diffraction grating. The optimization final results for finding the optimum parameters of VPH diffraction grating at the Bragg Superblaze case are shown in Table 4.4.

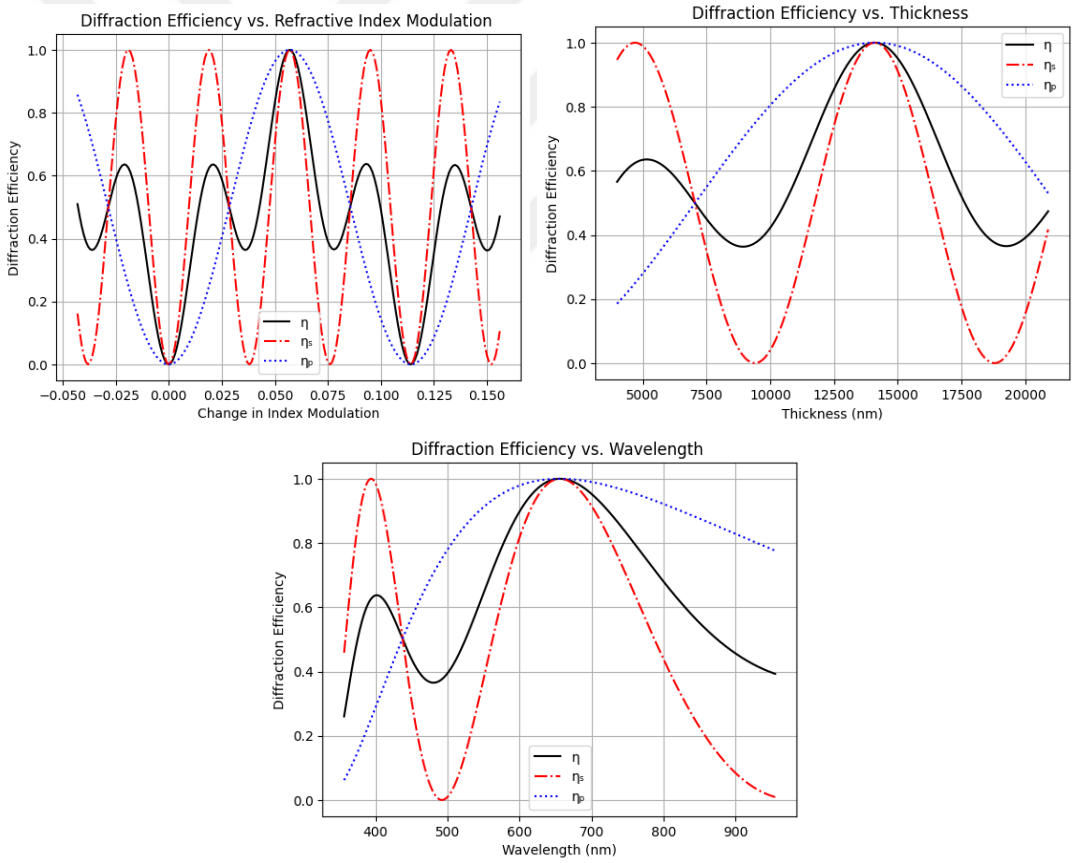


Figure 4.2: Red Arm diffraction efficiency: (top-left panel) With respect to the sinusoidal refractive index. (top-right panel) With respect to the grating thickness. (bottom panel) With respect to the wavelength.

Table 4.4: VPH Final Parameters for the NIR Arm. λ_c: Central Wavelength; $\Delta\lambda$: Wavelength Range; ν: Spatial Frequency; t: Grating Thickness; Δn: Sinusoidal Modulation; α: Blaze Angle.

λ_c (nm)	$\Delta\lambda$ (nm)	ν (lines/mm)	d (μm)	Δn	α (°)
1250	$1100 - 1400$	1240	19.9	0.099	50.81

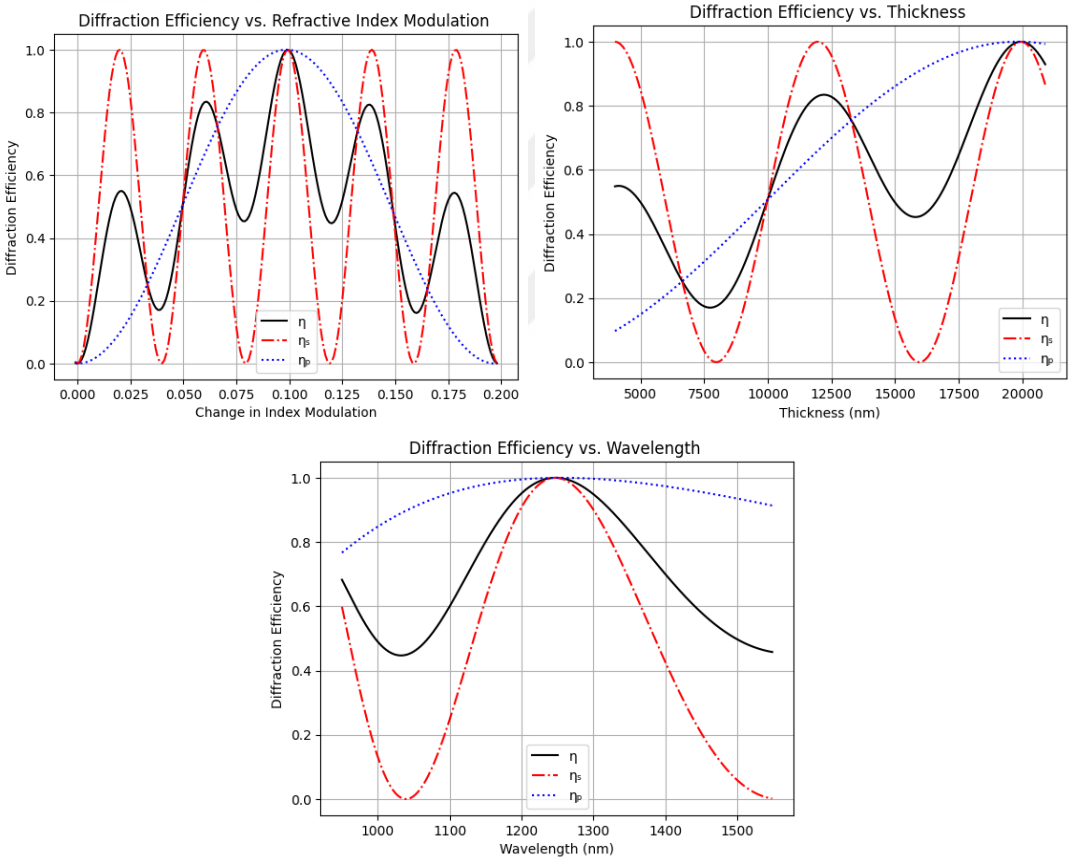


Figure 4.3: Near-Infrared (NIR) Arm diffraction efficiency: (top-left panel) With respect to the sinusoidal refractive index. (top-right panel) With respect to the grating thickness. (bottom panel) With respect to the wavelength.

CHAPTER 5

SPECTROGRAPH OPTICAL DESIGN

A spectrograph is an astronomical instrument that reproduces the image at object plane of its entrance slit. In this work, the entrance slit is a one-dimensional fiber array. At the image plane of the spectrograph, a CCD camera is used to detect the spectrum of the rays coming out of each fiber (see Figure 5.1).

In this context, vertical axis of the CCD camera gives information about spatial data and horizontal axis gives information about the spectrum obtained per each fiber. At the end of the observation, image reconstruction can be performed to recover the original spatial image by knowing the location of each fiber and its original position in the object space of the telescope.

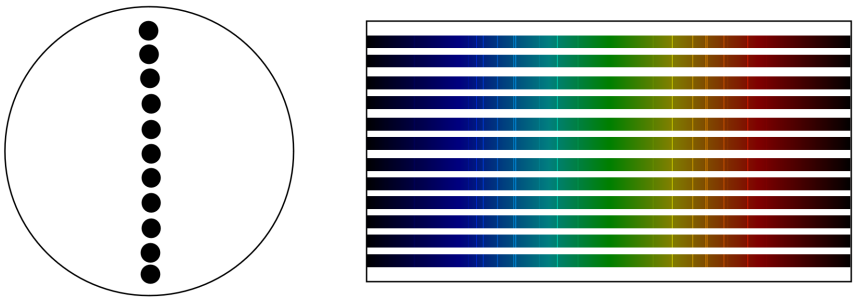


Figure 5.1: 1D fiber array slit (left) and dispersed spectra along spatial direction as seen by a CCD camera (right).

Table 5.1: Requirements for the desired spectrograph.

Specification	Value
CCD Format	4k×4k
CCD Pixel Size	15 μm
Spectral Resolution	>1000 (Intermediate)
Entrance Slit Size	610 μm
Fiber f-Number	f/3.4
Arms Number	3

5.1 Geometrical Optics Calculations

The first step in the design of the desired spectrograph is to calculate the optimum parameters of the collimator, grating and camera optics. These calculations are essentially an iterative process to find the best parameters that achieve intermediate spectral resolution for all the three arms. The spectral resolution (see equation 2.11) is restricted by the collimator focal length, diffraction order and line density of the grating, and it is inversely proportional to the size of the entrance slit.

In chapter 3, an extensive process was introduced in order to decrease the size of the entrance slit. In chapter 4, another calculation process was handled to find the best line density of the grating to achieve high optical throughput by calculating the diffraction efficiency of the VPH grating. In this chapter, to find the optimum optics of the collimator and camera based on the required parameters listed in Table 5.1, another calculation stage of the geometrical optics of the three arms design has been performed.

A comparison of how the variation of the focal length of the collimator will change in the diffraction limited Airy disk in the blue part of the spectrum and the values of the overall spectrograph is studied (see Figure 5.2). This study was made for the blue arm and similar results were found for the red and NIR arms. Therefore, the optimum focal length for the collimator was found at f_{coll}=550 mm for the three arms. Using the mathematics of the geometrical optics of the spectrograph mentioned in Chapter 2, the

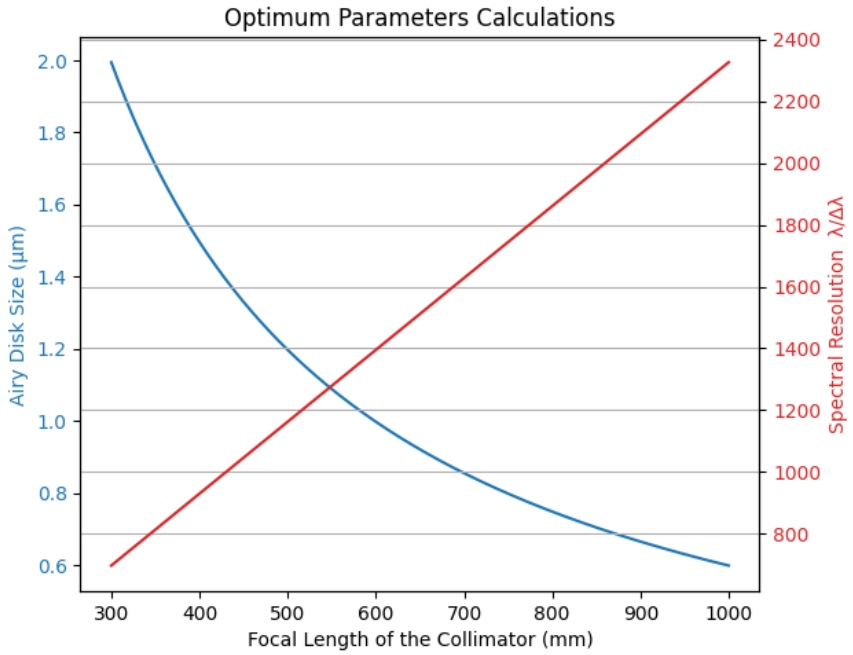


Figure 5.2: Variation in collimator focal length and the resulted spectral resolution and Airy disk.

other optical parameters of the grating and camera optics were calculated accordingly. The final spectral resolution ranges for all arms were found to fit properly for the intermediate spectral resolution range required. The final results of the calculations are given in Table 5.2.

Table 5.2: Optical system parameters for the three-arm design.

Arm	D_{coll} (mm)	f_{coll} (mm)	D_{cam} (mm)	f_{cam} (mm)	L_{grat} (mm)	Resolution Range
Blue	161.8	550	161.8	156.1	198.3	1105–1447
Red	161.8	550	161.8	93.0	198.2	1069–1594
NIR	161.8	550	161.8	90.8	255.9	1946–2477

CHAPTER 6

CONCLUSION

Imaging and spectroscopy are combined in Integral Field Units (IFU). The spectrograph design is based on using Volume-Phase Holographic gratings as the main dispersing elements. VPH gratings provide an outstanding diffraction efficiency, which is preferable in getting the spectroscopic data of faint celestial objects due to their high optical throughput. There are several methods for increasing the overall spectral resolution of the designed spectrograph such as increasing the focal length of the collimator, increasing the line density of the grating or decreasing the size of the entrance slit. One approach to increase the spectral resolution of a spectrograph is to increase the line/groove density. On the other hand, this leads to a narrower diffraction efficiency over a specific spectral range. It then leads to a multiple-arm approach to divide the spectral range into several spectral channels to maintain the spectral resolution for a specific range. In that way, the spectral resolution and the diffraction efficiency (optical throughput) could be controlled for the desired range.

In this design, RCWA calculations based on the first-order Kogelnik's approximation were made to find the optimum parameters of the VPH grating, leading to technical requirements of high optical throughput and moderate spectral resolution. In this work, three spectral arms are developed, namely blue, red and NIR spectral regions to cover the visible and near-infrared spectral ranges.

Several ways of dividing the FoV at the telescope's focal plane were tested for the IFUs designed in this work. The main constraint at this stage is the seeing limited disc. The best sampling method made for the final IFU is to divide the field to several segments and sample the seeing limited disc to a single microlens and further to a single fiber. This design would fit better to the adaptive optics side of the telescope

where the seeing limited disc is reduced. This design will lead to a wider coverage of the field of view at the telescope's focal plane. Following the recent developments in fiber optics, a fiber with a diameter of 10 microns was used to deploy images to the spectrograph's entrance slit. This small fiber diameter allows us to use a small diameter of a microlens, leading to the use of a telecentric demagnifier rather than a telecentric magnifier at the fore-optics side due to the size of the seeing limited disc.

Reducing the size of the entrance slit (w) dramatically increased the overall spectral resolution of the instrument. Therefore, a small core diameter fiber was a priority in technical requirements because using a small fiber at the IFU side will lead to a narrow aperture at the entrance slit leading to the desired spectral resolution range. For instance, in the initial design of the integral field unit (see Table 3.1), the number of fibers was high leading to a wide entrance slit in the spectrograph. Therefore an improved design was considered at that stage in order to reduce the entrance size which consequently led to a less complex design of the collimator and following optics.

Long entrance slits in spectrographs were also causing undesirable complexity in the optical design process. They usually degrade the overall resolving power of the instrument by decreasing the spectral resolution and causing several problems with collimating. Collimation is usually perfect for any on-axis field points. On the other hand, collimation of a longer slit gets complicated due to the necessity of using several optical elements to make all the light at all field points along the slit to be near-perfectly collimated i.e. parallel to the diffraction grating surface. These collimators usually require wide-field correctors before reaching to the grating surface.

Several methods were tested to divide the telescope's focal plane into segments to design the integral field unit. To decide about the suitable method one should follow four figures of merit: small slit size at the spectrograph's entrance, wider FOV coverage from the telescope side, high coupling efficiency through fibers and filling efficiency. Hexagonal packing showed the best filling option that reached close to 100% filling efficiency in our IFU design in using a hexagonal microlens array. On the other hand, using circular fiber arrays had a poor filling performance giving a filling efficiency of 47.5% (see Table 3.1).

After defining the scientific needs and technical requirements of the spectrograph a Python code was developed to compute the basic optical parameters of the VPH grating that provide high diffraction efficiency and cover the widest possible spectral range. The code also computes the basic parameters of geometrical optics of the spectrograph to find the optical parameters of the collimator, grating and camera optics that meet the technical requirements.

Finally, we tested and verified the results calculated for the geometrical optics of the collimator, grating and camera optics over OpticStudio/ZEMAX. It is found that the optical layout agrees with the results which are listed in Table 5.2.

Further optimization with real optics and performance test analyses will be required to carry on the study.

REFERENCES

[1] C. Yesilyaprak, O. Keskin, and L. Jolissaint, "Eastern anatolia observatory (dag): the status in 2022, towards the first light," in *Ground-based and Airborne Telescopes IX*, vol. 12182, pp. 330–341, SPIE, 2022.

[2] R. A. d. S. Ribeiro, *Optical Conceptual Design for the Giant Magellan Telescope Multi-Object Astronomical and Cosmological Spectrograph*. PhD thesis, Universidade de São Paulo.

[3] J. Allington-Smith, "Basic principles of integral field spectroscopy," *New Astronomy Reviews*, vol. 50, no. 4-5, pp. 244–251, 2006.

[4] S. C. Barden, "Review of fiber-optic properties for astronomical spectroscopy," in *Fiber optics in Astronomy III*, vol. 152, pp. 14–19, 1998.

[5] M. Zghal, H.-E. Bouali, Z. B. Lakhdar, and H. Hamam, "The first steps for learning optics: Ibn sahl's, al-haytham's and young's works on refraction as typical examples," in *Education and Training in Optics and Photonics*, p. ESB2, Optica Publishing Group, 2007.

[6] A. Tbakhi and S. S. Amr, "Ibn al-haytham: father of modern optics," *Annals of Saudi medicine*, vol. 27, no. 6, pp. 464–467, 2007.

[7] A. Mills, "Newton's prisms and his experiments on the spectrum," *Notes and Records of the Royal Society of London*, vol. 36, no. 1, pp. 13–36, 1981.

[8] J. B. Hearnshaw, *The analysis of starlight: one hundred and fifty years of astronomical spectroscopy*. CUP Archive, 1990.

[9] N. d. Tyson, *Astrophysics for People in a Hurry*. WW Norton & Company, 2017.

[10] B. B. Nath and B. B. Nath, "The folklore and reality of the discovery of helium," *The Story of Helium and the Birth of Astrophysics*, pp. 249–268, 2013.

[11] G. R. KIRCHHOFF, "Chemical analysis by spectral observations," *Ann. d. Phys.*, vol. 110, p. 160, 1860.

[12] B. W. Carroll and D. A. Ostlie, *An introduction to modern astrophysics*. Cambridge University Press, 2017.

[13] S. A. Smee and G. J. Hill, "Ground-based astronomical instrumentation development in the united states: A white paper on the challenges faced by the us community," *arXiv preprint arXiv:2112.00957*, 2021.

[14] M. S. Bessell, "Standard photometric systems," *Annu. Rev. Astron. Astrophys.*, vol. 43, pp. 293–336, 2005.

[15] J. Binney and M. Merrifield, *Galactic astronomy*. Princeton University Press, 1998.

[16] D. W. Weedman, "Emission line galaxies," *Vistas in Astronomy*, vol. 21, no. 1, pp. 55–70, 1977.

[17] R. C. Kennicutt Jr, "The rate of star formation in normal disk galaxies," *Astrophysical Journal, Part 1 (ISSN 0004-637X), vol. 272, Sept. 1, 1983, p. 54-67.*, vol. 272, pp. 54–67, 1983.

[18] Y. Qiu, T. Bogdanović, Y. Li, and M. McDonald, "Using hα filaments to probe active galactic nuclei feedback in galaxy clusters," *The Astrophysical Journal Letters*, vol. 872, no. 1, p. L11, 2019.

[19] X. Fan, "Evolution of high-redshift quasars," *New Astronomy Reviews*, vol. 50, no. 9-10, pp. 665–671, 2006.

[20] S. Persson, D. Murphy, W. a. Krzeminski, M. Roth, and M. Rieke, "A new system of faint near-infrared standard stars," *The Astronomical Journal*, vol. 116, no. 5, p. 2475, 1998.

[21] R. A. Ribeiro, D. Jones, L. M. Schmidt, K. Taylor, E. Cook, D. L. DePoy, D. Faes, C. Froning, T.-G. Ji, H.-I. Lee, *et al.*, "Optical design for the giant magellan telescope multi-object astronomical and cosmological spectrograph (gmacs): design methodology, issues, and trade-offs," in *Optical Design and Engineering VII*, vol. 10690, pp. 562–575, SPIE, 2018.

[22] J. W. Hardy, "Active optics: a new technology for the control of light," *Proceedings of the IEEE*, vol. 66, no. 6, pp. 651–697, 1978.

[23] R. Zhelem, R. Content, V. Churilov, Y. Kripak, L. Waller, S. Case, S. Mali, R. Muller, M. Gonzalez, D. Adams, *et al.*, "Design of the near infrared camera dirac for east anatolia observatory," in *Ground-based and Airborne Instrumentation for Astronomy IX*, vol. 12184, pp. 1301–1312, SPIE, 2022.

[24] O. Keskin, L. Jolissaint, A. Bouxin, and C. Yesilyaprak, "Troia adaptive optics system for dag telescope: assembly and laboratory performance prior to on-sky assessment," in *Adaptive Optics Systems VIII*, vol. 12185, pp. 567–578, SPIE, 2022.

[25] O. Keskin, S. K. Yerli, C. Yeşilyaprak, T. Guver, S. Aliş, F. K. Yelkenci, B. B. Güçsav, M. Ö. O. Arabaci, and A. Erol, "Status of focal plane instrumentation (fpi) project of the 4m dag telescope," in *Ground-based and Airborne Instrumentation for Astronomy VI*, vol. 9908, pp. 1642–1647, SPIE, 2016.

[26] W. Shi, L. Gao, L. Zhang, Z. Feng, F. Fang, and G. Xia, "The evaluation of spectral resolution in the optical design of a czerny-turner spectrometer," in *Photonics*, vol. 9, p. 678, MDPI, 2022.

[27] E. Pearson and C. Rathmell, "Vph transmission grating design considerations for spectrograph designers," in *Advances in Optical and Mechanical Technologies for Telescopes and Instrumentation V*, vol. 12188, pp. 738–746, SPIE, 2022.

[28] Y. Zhang, W. Li, W. Duan, Z. Huang, and H. Yang, "Echelle grating spectroscopic technology for high-resolution and broadband spectral measurement," *Applied Sciences*, vol. 12, no. 21, p. 11042, 2022.

[29] J. Hang-xin, H. Zhong-wen, Z. Yong-tian, X. Ming-ming, D. Song-xin, Z. Hua-tao, T. Zhen, and W. Jin-feng, "Wide field multi-object spectrograph for 30 m class optical/near-infrared telescopes," *Chinese Astronomy and Astrophysics*, vol. 43, no. 4, pp. 493–518, 2019.

[30] H. Zhang, W. Wang, S. Yip, D. Li, F. Li, C. Lan, F. Wang, C. Liu, and J. C. Ho, "Enhanced performance of near-infrared photodetectors based on ingaas

nanowires enabled by a two-step growth method," *Journal of Materials Chemistry C*, vol. 8, no. 47, pp. 17025–17033, 2020.

[31] A. M. Karmalawi and A. A. Abdelmageed, "Development of a detector-based absolute spectral power responsivity scale in the spectral range of 300–1600 nm," *Journal of Materials Science: Materials in Electronics*, vol. 32, no. 4, pp. 5215–5221, 2021.

[32] G. Cottrell, *Observational Astronomy: A Very Short Introduction*. Oxford University Press, 2023.

[33] J. Sasián, *Introduction to lens design*. Cambridge University Press, 2019.

[34] M. Birjukovs, A. Jegorovs, A. Jakovics, A. Klokovs, and I. Felcis, "Design optimization automation for luminaire reflectors using comsol multiphysics and performance comparison against zemax opticstudio," in *2019 XXI International Conference Complex Systems: Control and Modeling Problems (CSCMP)*, pp. 208–213, 2019.

[35] J. B. Dos Santos, A. C. De Oliveira, J. Gunn, L. S. De Oliveira, M. V. De Arruda, B. Castilho, C. D. Gneiding, F. F. Ribeiro, G. Murray, D. J. Reiley, *et al.*, "Studying focal ratio degradation of optical fibers for subaru's prime focus spectrograph," in *Advances in Optical and Mechanical Technologies for Telescopes and Instrumentation*, vol. 9151, pp. 1703–1708, SPIE, 2014.

[36] J. Lin, N. Jovanovic, and M. P. Fitzgerald, "Design considerations of photonic lanterns for diffraction-limited spectrometry," *JOSA B*, vol. 38, no. 7, pp. A51–A63, 2021.

[37] I. K. Baldry, J. Bland-Hawthorn, and J. Robertson, "Volume phase holographic gratings: polarization properties and diffraction efficiency," *Publications of the Astronomical Society of the Pacific*, vol. 116, no. 819, p. 403, 2004.

[38] X.-t. Yan, J.-f. Yang, B. Xue, X.-l. Ma, F. Li, Y.-y. Zhao, and F. Bu, "Design of the microlens arrays coupling with imaging fiber bundle," *Optoelectronics Letters*, vol. 9, no. 3, pp. 169–172, 2013.